Cell Reports

Article

Regulation of the BCR signalosome by the class II peptide editor, H2-M, affects the development and repertoire of innate-like B cells

Graphical abstract

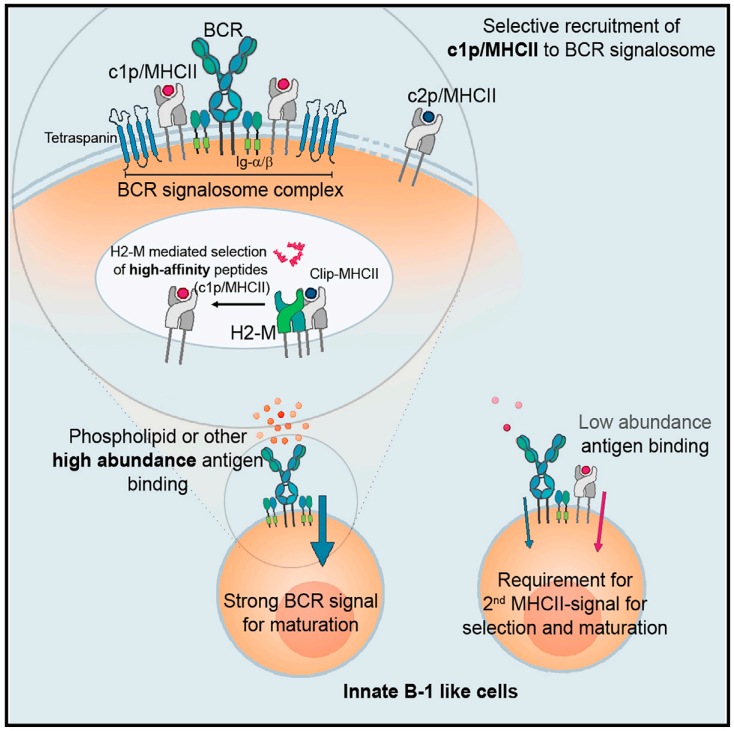

Highlights

- H2-M deficiency reduces B-1a cell self-renewal and cell survival
- Lack of H2-M:MHCII interaction leads to a neonatal-like B-1a cell clonal repertoire
- H2-M loss reduces plasma membrane association of p/MHCII with BCRs
- H2-M selection of MHCII peptide cargo regulates BCR signalosome signal intensity

Authors

Debopam Ghosh, Tho D. Pham, Padma P. Nanaware, ..., Scott D. Boyd, Eliver E.B. Ghosn, Elizabeth D. Mellins

Correspondence

dghosh23@stanford.edu (D.G.), eliver.ghosn@emory.edu (E.E.B.G.), mellins@stanford.edu (E.D.M.)

In brief

H2-M is an MHCII peptide editor that selects for stable peptide-MHCII complexes. Ghosh et al. show that H2-M loss reduces plasma membrane p/MHCII:BCR association and BCR signal strength, highlighting a mechanism by which B-1a cell clonal selection and development directly depend on the functional association of H2-M with MHCII.

Ghosh et al., 2022, Cell Reports *38*, 110200
January 25, 2022
https://doi.org/10.1016/j.celrep.2021.110200

CellPress

Cell Reports

CellPress
OPEN ACCESS

Article

Regulation of the BCR signalosome by the class II peptide editor, H2-M, affects the development and repertoire of innate-like B cells

Debopam Ghosh,[1,*] Tho D. Pham,[2] Padma P. Nanaware,[6] Deepanwita Sengupta,[3] Lital N. Adler,[1,10] Caiyun G. Li,[4] Xiao He,[7] Mary E. O'Mara,[8] Aaron B. Kantor,[5] Khoa D. Nguyen,[2] Yang Yang,[5] Laurence C. Eisenlohr,[8] Peter E. Jensen,[7] Leonore A. Herzenberg,[5] Lawrence J. Stern,[6] Scott D. Boyd,[2] Eliver E.B. Ghosn,[9,11,*] and Elizabeth D. Mellins[1,11,12,*]

[1]Department of Pediatrics, Stanford University, Stanford, CA 94305, USA
[2]Department of Pathology, Stanford University, Stanford, CA 94305, USA
[3]Department of Biology, Stanford University, Stanford, CA 94305, USA
[4]Department of Radiation Oncology, Stanford University, Stanford, CA 94305, USA
[5]Department of Genetics, Stanford University, Stanford, CA 94305, USA
[6]Department of Pathology, University of Massachusetts Medical School, Worcester, MA 01605, USA
[7]Department of Pathology, University of Utah, Salt Lake City, UT 84112, USA
[8]Department of Pathology and Laboratory Medicine, Children's Hospital of Philadelphia Research Institute and University of Pennsylvania Perelman School of Medicine, Philadelphia, PA 19104, USA
[9]Departments of Medicine and Pediatrics, Lowance Center for Human Immunology, Emory Vaccine Center, Emory University School of Medicine, Atlanta, GA 30322, USA
[10]Present address: Weizmann Institute of Science, Rehovot, Israel
[11]Senior author
[12]Lead contact
*Correspondence: dghosh23@stanford.edu (D.G.), eliver.ghosn@emory.edu (E.E.B.G.), mellins@stanford.edu (E.D.M.)
https://doi.org/10.1016/j.celrep.2021.110200

SUMMARY

The non-classical Major Histocompatibility Complex class II (MHCII) protein, H2-M, edits peptides bound to conventional MHCII in favor of stable peptide/MHCII (p/MHCII) complexes. Here, we show that H2-M deficiency affects B-1 cell survival, reduces cell renewal capacity, and alters immunoglobulin repertoire, allowing for the selection of cells specific for highly abundant epitopes, but not low-frequency epitopes. H2-M-deficient B-1 cells have shorter CDR3 length, higher content of positively charged amino acids, shorter junctional regions, less mutation frequency, and a skewed clonal distribution. Mechanistically, H2-M loss reduces plasma membrane p/MHCII association with B cell receptors (BCR) on B-1 cells and diminishes integrated BCR signal strength, a key determinant of B-1 cell selection, maturation, and maintenance. Thus, H2-M:MHCII interaction serves as a cell-intrinsic regulator of BCR signaling and influences the selection of the B-1 cell clonal repertoire.

INTRODUCTION

B cells play a unique role as antigen-presenting cells (APCs) to $CD4^+$ T cells by privileging presentation of antigens recognized by B cell receptors (BCRs). Reciprocally, the T cell receptor for antigen (TCR):peptide/ Major Histocompatibility Complex class II (MHCII) complex (p/MHCII) interaction provides an activation signal to B cells. BCR-bound protein antigen is delivered by internalized BCR to late endosomal compartments, where the antigen is processed to smaller peptide fragments that are bound to MHCII. The non-classical MHCII protein, H2-M (HLA-DM in humans), regulates by selecting and loading high-affinity peptides onto MHCII proteins (Denzin and Cresswell, 1995; Sloan et al., 1995). H2-M removes the "place holder" peptide, class II invariant chain peptide (CLIP), from the MHCII peptide-binding groove, and also selects for tight-binding peptides (Pos et al., 2013). Allelic differences in MHCII affect affinities for CLIP peptide (Doebele et al., 2003; Sette et al., 1995) and for H2-M (Fallang et al., 2008; Zhou et al., 2016), with consequences for peptide selection. H2-M also interacts with another class II-like protein, H2-O, which most evidence argues acts as a competitive inhibitor of H2-M (Guce et al., 2013; Liljedahl et al., 1998). H2-M editing of p/MHCII complexes as a regulator of selection and proliferation of $CD4^+$ T cells has been studied widely. However, less attention has been paid to effects of H2-M deficiency on APC.

BCR-derived activation signals play various roles in the selection and maintenance of B cell populations. This is particularly true for B-1 cell development, which unlike the ontogeny of adult bone-marrow-derived B (B-2 or follicular B) cells, occurs predominantly at early stages of life and is positively regulated by BCR affinity for self-antigen (Hayakawa et al., 1999). B-1 cell

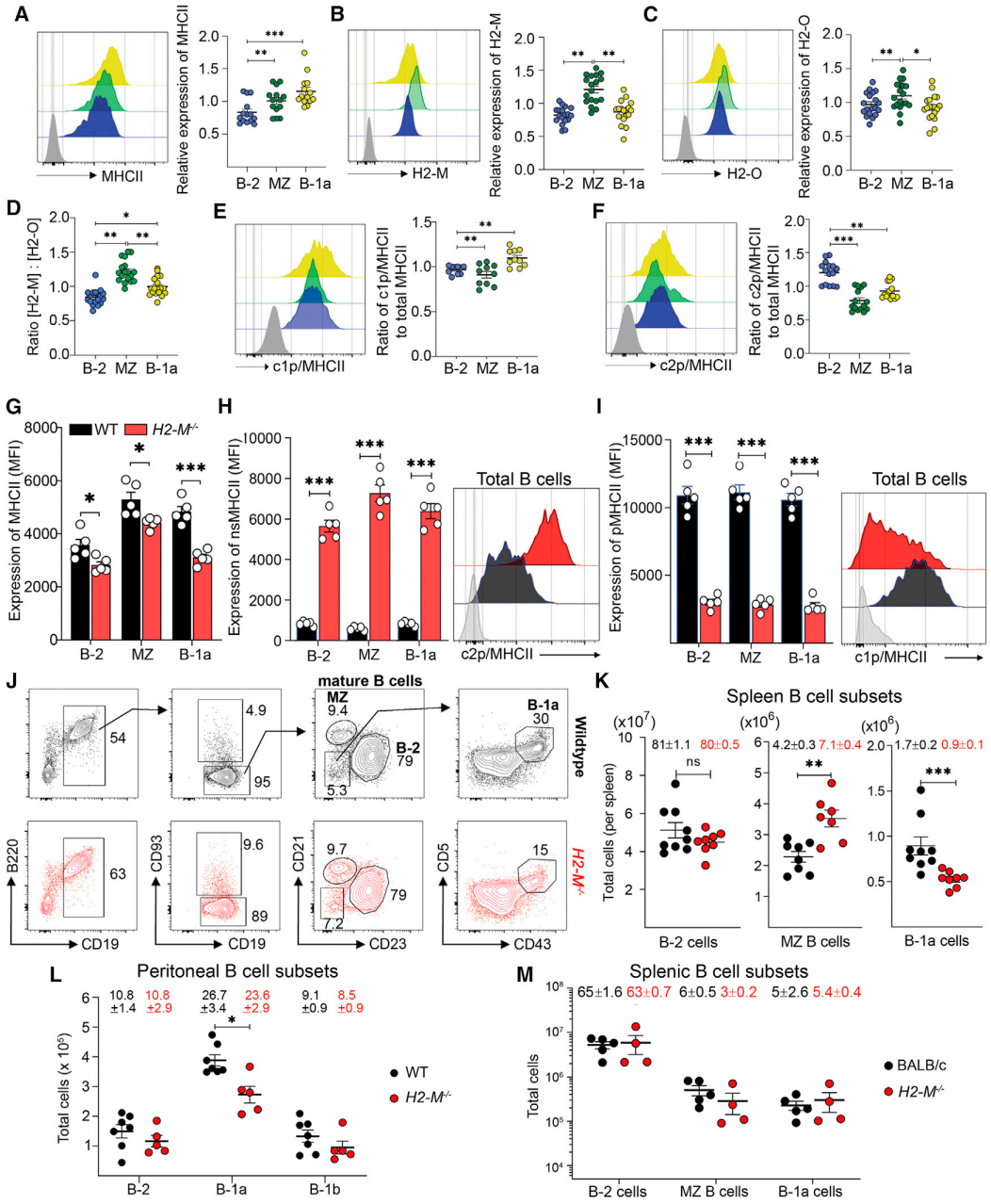

Figure 1. Absence of H2-M alters MHCII protein expression in B cells, and altered H2-M-MHCII interaction regulates the B-1 cell development in the secondary lymphoid organs of B6 mice

(A–C) (A) Histogram plot showing surface expression and scatterplot showing normalized median fluorescent intensity (MFI) of MHCII (I-A/I-E) by follicular (B-2) B cells (blue), MZ B cells (green), and splenic B-1a cells (yellow) from WT B6 mice. Fluorescent-minus-one (FMO) control for the total B cells is depicted in gray. Relative MFI was calculated by subtracting the MFI value of the same cell subset from the FMO control sample. Histogram plot showing expression and scatterplot showing normalized MFI of intracellular expression of (B) H2-M and (C) H2-O by splenic B-2, MZ, and B-1a cells from WT B6 mice. Normalization was done by subtracting the MFI value of the FMO control for the corresponding cell population.

(D–F) (D) Scatterplot showing net H2-M function in splenic B cell subsets by plotting the ratio of intracellular H2-M to H2-O MFI. Histogram plot showing expression and scatterplot showing normalized expression of (E) c2p/MHCII (non-specific-peptide complexed with I-A^b, 15G4 clone) and (F) c1p/MHCII (productive peptide-I-A^b complex, KH74 clone) by splenic B-2, MZ, and B-1a cells from WT B6 mice. Relative expression of c2p/MHCII and c1p/MHCII was calculated by normalizing against MFI of total MHCII expression by the corresponding B cell subsets. Data (A–F) are pooled from three individual experiments,

(legend continued on next page)

development starts during embryogenesis and peaks during fetal and neonatal life to contribute significantly to the adult B-1 cell pool (Ghosn et al., 2019). B-1 cells are characterized by their low B220 expression and IgM^{hi}CD19^{hi}CD23^{-}CD43^{+} phenotype (Hardy and Hayakawa, 2001); they are derived from a B-1-specific precursor population, identified by Lin^{-}Ig^{-}CD19^{+} B220$^{lo/-}$CD93^{+} (Ghosn et al., 2011; Montecino-Rodriguez et al., 2006, 2016). In adults, B-1 cells are seldom replenished from bone-marrow-derived progenitors (Esplin et al., 2009), but rely mostly on self-renewal (Casola et al., 2004; Kobayashi et al., 2020) to maintain the pool (reviewed in (Baumgarth, 2017).

Factors influencing B-1 cell development are incompletely understood. However, evidence supports B-1a (CD5^{+} B-1) cells as a separate lineage that requires positive selection, relying on high BCR affinity for antigen (Ghosn et al., 2019). B-1a cell differentiation is impaired if mutations abrogate BCR signal strength (Khan et al., 1995; Zhang et al., 1995). The absence of negative regulators of BCR signaling enhances the B-1a cell pool (Chan et al., 1997). The majority of B-1a BCRs are polyreactive, recognizing self- and bacteria-derived carbohydrate and lipid for homeostasis and broad-spectrum immunity, respectively (Baumgarth, 2011; Forster and Rajewsky, 1987). A considerable proportion of murine B-1a cells carry BCRs specific for phosphatidylcholine (PtC) and phosphorylcholine (PC), which help in the clearance of apoptotic cells (Gronwall et al., 2012; Shaw et al., 2003).

Here, we analyzed B cell development in H2-M-deficient mice. We uncovered effects on development and BCR repertoire of the B-1 cell lineage. Mechanistically, we showed that H2-M-selected p/MHCII complexes make a critical contribution to the integrated BCR signal required for normal B-1a cell development and repertoire.

RESULTS

Expression of H2-M and MHCII protein cargo in B cell lineages

We observed higher MHCII protein (I-A^{b}) surface expression on splenic B-1a versus B-2 (follicular) cells (Figure 1A) and on peritoneal B-1 versus B-2 cells (Figure S1C). The H2-M:H2-O ratio, indicating levels of free, functional H2-M, was highest in marginal zone (MZ) B cells, intermediate in splenic B-1a cells, and lowest in B-2 cells (Figure 1D). Splenic B-1a cells had the highest level of conformer 1 peptide-MHCII (c1p/MHCII) complexes, defined by binding of mAb KH74 (Figure 1E). Consistent with their free H2-M level, MZ B cells had the lowest surface level of I-A^{b} conformers with apparently non-edited peptides, such as CLIP (c2p/MHCII; conformer 2), defined by binding of mAb 15G4 (Figure 1F) (Liljedahl et al., 1998).

In *H2-M*$^{-/-}$, but not *H2-O*$^{-/-}$, B6 mice, total B cell surface I-A^{b} (binding of mAb M5/114) was reduced compared with wild-type (WT) mice (Figures 1G, S2A, S2D, and S2E). This difference was detected after the early stages of development (pre-pro- and pro-B) in the bone marrow, when MHCII expression increases (Hayakawa et al., 1994). Reduced I-A^{b} in *H2-M*$^{-/-}$ mice is likely linked to preferential ubiquitination and internalization of MHCII-CLIP (and other conformer 2 complexes) compared with peptide-MHCII (conformer 1) complexes (Ishido and Kajikawa, 2019) or to the chaperoning effects of H2-M (Kropshofer et al., 1997). As expected, all B cell subsets from *H2-M*$^{-/-}$ I-A^{b} mice displayed MHCII predominantly in c2p/MHCII (Figure 1H), rather than c1p/MHCII (Figure 1I).

H2-M regulates B-1 cell numbers in secondary lymphoid organs

H2-M loss in B6 mice did not significantly affect the frequencies of precursor B cells (pre-pro-, pro-, and pre-B cells), immature (CD93^{+}IgD^{-}IgM^{+}) B cells, and mature B-2 cells in bone marrow or spleen (Figures 1J, 1K, S3A, and S3B). However, H2-M deficiency resulted in ~48% decrease in absolute numbers of splenic B-1a cells, ~68% increase in MZ B cells (Figures 1J and 1K), and ~30% decrease in peritoneal B-1a, but not B-1b, cells (Figure 1L). These changes did not simply correlate with the level of I-A^{b}, as complete absence of MHCII (*MHCII*$^{-/-}$) did not further decrease splenic B-1a cell frequency (Figures S3C–S3E). Compared with *H2-M*$^{-/-}$ mice, *MHCII*$^{+/-}$ (heterozygous) mice had increased splenic B-1a cells, despite lower MHCII levels (Figures S3C–S3E), but also had higher c1p/MHCII levels (Figure S3E). In *H2-O*$^{-/-}$ mice (higher active H2-M), both splenic B-1a cell frequency and c1p/MHCII levels were increased above WT (Figures S3C–S3E, and S3G). Taken together, these data imply that DM-dependent expression of c1p/MHCII conformers, rather than MHCII level per se, is critical to maintaining B-1 cell numbers in B6 mice.

with n = 3–4 mice/group; representative histogram plots are accompanied. *, $p < 0.05$, **, $p < 0.01$, ***, $p < 0.005$ (one-way ANOVA followed by Tukey's multiple comparisons).

(G–I) (G) Bar graphs showing the surface expression of MHCII (clone M5/114.15.2) by B cell subsets from spleens of WT (Black) and *H2-M*$^{-/-}$ (red) mice. Splenic B-2 cells (CD19^{+}B220^{+}CD23^{+}CD21^{int}), MZ B cells (CD19^{+}B220^{+}CD23^{-}CD21^{hi}), and B-1a cells (CD19^{hi}B220^{lo}CD23^{-}CD21^{-}IgM^{hi}CD43^{+}CD5^{+}) from spleen were pre-gated using the above-mentioned markers by flow cytometry. Bar graphs showing surface expression of (H) c2p/MHCII and (I) c1p/MHCII by splenic B-2, MZ, and B-1a cells from WT (black) and *H2-M*$^{-/-}$ (red) mice. Corresponding histogram plots showing expression of c2p/MHCII and c1p/MHCII by splenic B cells from WT (black) and *H2-M*$^{-/-}$ (red) B6 mice, FMO control depicted in gray. ***, $p < 0.005$, ****, $p < 0.001$ (multiple *t* test one per row). Data (G–J) representative of two individual experiments, with n = 5 mice/groups.

(J) Representative flow plots indicating general gating strategy for selection of B-2 B cells, MZ B cells, and B-1a cells (live CD19^{hi}B220$^{+/lo}$ CD23^{-}CD21^{-}CD43^{+}CD5^{+}) from the spleens of WT (black) and *H2-M*$^{-/-}$ (red) mice; each contour plot shows 8,000 events.

(K) The total number of B-2 cells, MZ B cells, and B-1a cells from the spleens of WT and *H2-M*$^{-/-}$ mice from C57BL/6 background. Percentages of total splenic B cells are provided in the number above corresponding B cell subsets as mean ± SEM.

(L) The total number of B-2, B-1a, and B-1b cells from the peritoneum of WT and *H2-M*$^{-/-}$ mice from C57BL/6 background. Percentages of total peritoneal cells are provided in the number above corresponding B cell subsets as mean ± SEM.

(M) The total number of B-2, MZ, and B-1a B cells from the spleens of WT and *H2-M*$^{-/-}$ mice from BALB/c background. Percentages of total splenic B cells are provided in the number above corresponding B cell subsets as mean ± SEM. *, $p < 0.05$, **, $p < 0.01$, ***, $p < 0.005$ (non-parametric Mann-Whitney test). Data (K–M) are representative of or pooled from two individual experiments with n = 4–5 mice/group. All the bar graphs or scatterplots are presented as mean ± SEM.

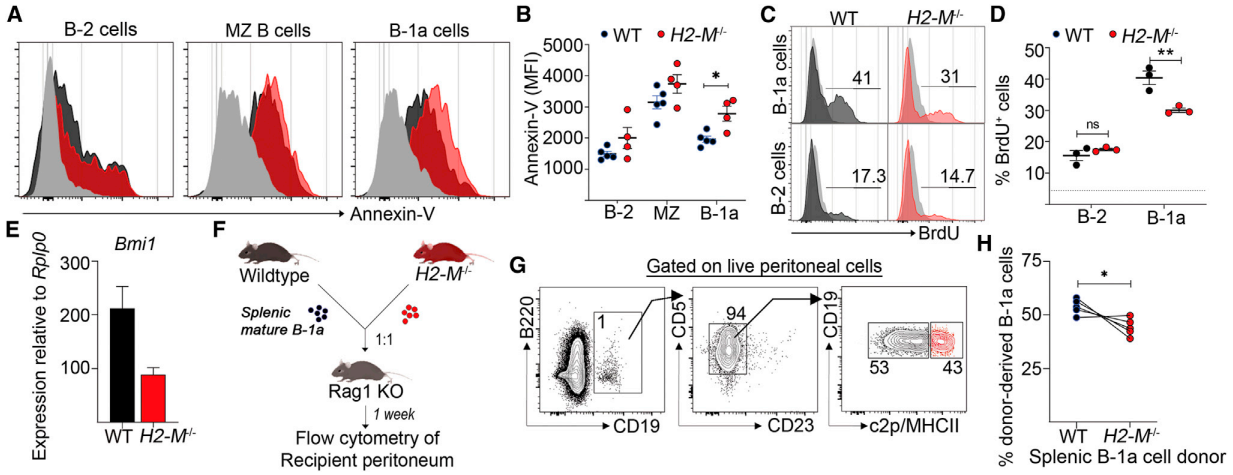

Figure 2. Absence of H2-M affects B-1 cell survival and renewal abilities

(A) Representative histogram plots indicating mature B-2 B cells, MZ B cells, and B-1a cells from the spleens of WT and *H2-M*$^{-/-}$ mice showed labeling with Annexin-V. Corresponding FMO controls depicted as gray.

(B) The expression of Annexin-V by B-2 cells, MZ B cells, and B-1a cells (MFI) from the spleens of WT C57BL/6 (black) and *H2-M*$^{-/-}$ mice (red).

(C) Adult WT and *H2-M*$^{-/-}$ mice were fed with 0.8 mg/mL BrdU in drinking water along with 1% sucrose for six days before harvesting and analysis of the tissues. Representative histogram plots indicating BrdU incorporation of mature B-2 cells and B-1a cells from WT (black) and *H2-M*$^{-/-}$ mice (red) from C57BL/6 background. Mice not treated with BrdU served as background control and shown as a gray histogram.

(D) Percentages of B-2 cells and B-1a cells incorporating BrdU from the spleens of WT and *H2-M*$^{-/-}$ mice. Each dot represents an individual animal. **, $p < 0.01$ (multiple *t* test).

(E) Expression of *Bmi1* at the transcript level relative to the expression of *Rplp0* by mature B-1a cells from WT (black) and *H2-M*$^{-/-}$ (red) mice.

(F) Mature splenic B-1a cells from WT and *H2-M*$^{-/-}$ mice were FACS-purified, mixed in 1:1 ratio, and transferred intraperitoneally in *Rag1*$^{-/-}$ mice. The peritoneal exudates from recipient mice were analyzed by flow cytometry one week following transfer.

(G) Representative flow plots showing the donor-derived CD19^{+} population and their phenotype.

(H) Scatterplot indicating the percentage of donor-derived B-1a cells developed from WT congenic (black) and H2-M-deficient donor (red) mice. Each point indicates an individual animal. *, $p < 0.05$ (Wilcoxon matched-pairs signed rank test). Data represent one independent experiment with n = 3–5 mice/group. All the bar graphs or scatterplots are presented as mean ± SEM.

H2-M regulates B-1 cell survival

A small but significant increase in the proportion of apoptotic mature splenic B-1a cells, but not B-2 or MZ B cells, was observed in *H2-M*$^{-/-}$ compared with WT B6 mice (Figures 2A and 2B). As B-1a cells replenish through self-renewal, we tested their proliferative capacity by BrdU incorporation. WT B-1a cells showed increased BrdU accumulation compared with *H2-M*$^{-/-}$ B-1a cells (Figures 2C and 2D). WT cells also had higher polycomb group protein Bmi1 mRNA, critical for B-1 cell self-renewal (Kobayashi et al., 2020) (Figure 2E). As another approach, we fluorescence-activated cell sorting (FACS)-purified mature splenic B-1a cells (CD19^{+}B220^{lo}IgM^{+}CD93^{-}CD23^{-}CD43^{+}CD5^{+}) from WT and *H2-M*$^{-/-}$ mice, mixed them 1:1, and transferred the cells intraperitoneally into *Rag*-deficient mice (Figure 2F). WT B-1a cells (c2p/MHCII^{lo}) showed a survival advantage over the *H2-M*$^{-/-}$ (c2p/MHCII^{hi}) B-1a cells (Figures 2G and 2H). Thus, H2-M deficiency reduces splenic B-1a cell numbers by increased death and decreased self-renewal.

H2-M promotes differentiation of B-1 cells

Lower numbers of mature B-1 cells in *H2-M*$^{-/-}$ mice also could reflect reduced differentiation of B-1 precursors. We found significant reductions in B-1 cell precursors (Lin^{-}B220$^{-/lo}$ sIg^{-}CD19^{+}CD93^{+}; Figure S4A) in E18.5 fetal liver in *H2-M*$^{-/-}$ mice versus WT [(Figure 3A; but not detectably in spleen post-birth (Figure S4B)], and 2–3-w-old *H2-M*$^{-/-}$ mice showed significantly reduced frequency and abundance of splenic transitional B-1a (CD93^{+}CD19^{+} IgM^{hi}IgD^{-}CD43^{+}CD5^{+}) and mature B-1a (CD93^{-}CD19^{+}B220^{lo}CD23^{-}CD21^{-}CD43^{+}CD5^{+}) cells compared with age-matched WT mice (Figures 3B and 3C).

H2-M$^{-/-}$ (vs WT) B-1 precursors (E18.5 liver or spleen) also had significantly reduced surface MHCII (total I-A^{b} and c1p/MHCII complex) (Figures S4C–S4E). As fetal B-1 precursors have low levels of all MHCII proteins (Tung et al., 2006), we used neonatal splenic B-1 precursors to determine when MHCII and H2-M levels increase. Following little to no expression at 1 week of age, the B-1 precursors showed a gradual and steady increase in MHCII and H2-M levels (Figure 3D) that peaked in adult mice (weeks 6–8). (A contribution of B-2 progenitors to the gated population over time cannot be ruled out). The timing of the increase in H2-M:H2-O ratio and c1p/MHCII levels on WT B-1 precursors (Figures 3E and 3F) matched the timing of reductions in transitional and mature B-1a cells in *H2-M*$^{-/-}$ mice. Sca-1 expression, which indicates differentiation potential (Morcos et al., 2017), was acquired in the same time frame (Figure 3G). Strikingly, as early as week one post-birth, splenic B-1 precursors acquired intracellular Ig-α and Ig-β (Figure 3G), which form the heterodimeric transducer of p/MHCII signaling (Lang

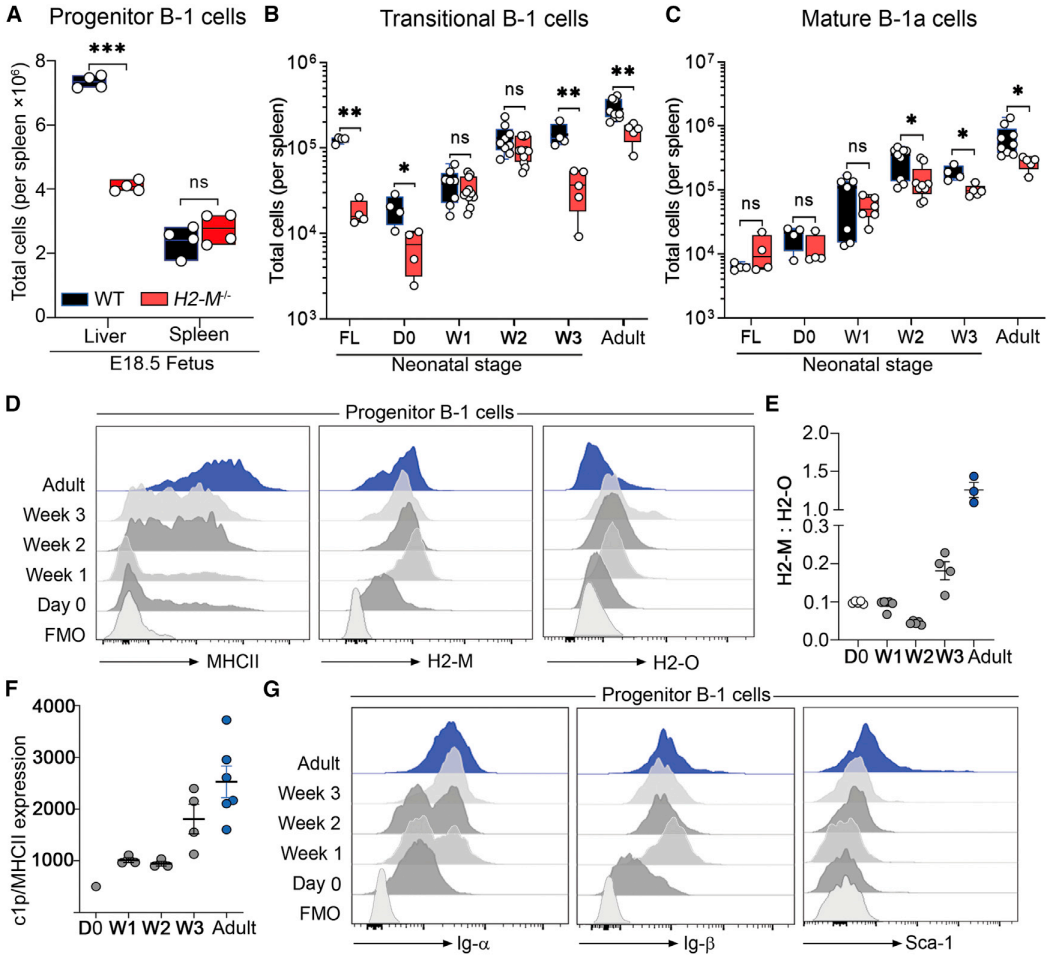

Figure 3. H2-M-MHCII interaction influences B-1 cell development following birth

(A–C) The total number of (A) B-1 cell precursors from E18.5 fetal liver and spleen of WT (black) and *H2-M*$^{-/-}$ mice (red), (B) transitional B-1a cells, and (C) mature B-1a cells from the spleen of WT (black) and *H2-M*$^{-/-}$ mice (red) day 0, weeks 1, 2, 3, and adult (6–8 weeks of age). B-1 cell precursors (Lin^{-}surface Ig^{-}CD19^{+}CD93^{+}B220$^{lo/-}$) (Ghosn et al., 2011), immature B-1a (CD19^{+}CD93^{+}CD5^{+}CD23^{-}IgM^{hi}), and mature B-1a (CD19^{+}B220$^{lo/-}$CD93^{-}CD43^{+}CD5^{+}CD23^{-}). ns = non-significant, *, $p < 0.05$, **, $p < 0.01$, two-way ANOVA, Sidak's multiple comparison test. Data representative of one (A) or pooled from five (B, C) individual experiments with n = 4–5 mice/group. The difference is more pronounced in the mature B-1a cell compartment, possibly due to the log-fold higher number of mature compared with transitional B-1a cells.

(D–F) (D) Representative histogram plots indicating expressions of surface MHCII, intracellular H2-M, and H2-O on B-1 precursors at different stages of development following birth from the spleens of WT C57BL/6 mice. Scatterplots showing (E) ratio of intracellular H2-M and H2-O (H2-M inhibitor) expressions and (F) expression of surface c1p/MHCII by B-1 precursors from the spleen of WT C57BL/6 mice.

(G) Representative histogram plots indicating intracellular expression of Ig-α and Ig-β and surface expression of activation marker "stem cell antigen (Sca-1)," on B-1 precursors at different stages of development following birth from the spleens of WT C57BL/6 mice. Each point indicates an individual animal. *, $p < 0.05$, **, $p < 0.01$ (multiple *t* test one per row). Data (D-G) representative of two independent experiments with n = 3–4 mice/group. All the scatterplots are presented as mean ± SEM.

et al., 2001). These data raised the possibility that MHCII-mediated signals regulate early stages of B-1 cell development, in an H2-M-dependent manner (see below).

To further explore H-2M's role in B-1 maturation, we adoptively transferred FACS-sorted B-1 precursors (Lin^{-}CD19^{+-}B220$^{lo/-}$CD93^{+}sIg^{-}) from 1-week-old WT (CD45.1^{+}) and *H2-M*$^{-/-}$ (CD45.2^{+}) mice, mixed 1:1, into *Rag1*$^{-/-}$ mice (Figure 4A). WT donor cells were most efficient at generating mature B-1a cells, whereas *H2-M*$^{-/-}$ donor cells appeared halted at the immature stage (Figures 4B–4D). In the peritoneum of recipient mice, WT donor cells made a significant preferential contribution to B-1a, but not B-1b, cells (Figures 4E–4G). Thus, our results argue that H2-M absence significantly limits the differentiation of B-1 precursors into mature B-1a cells. As co-transfer of CD4^{+} T cells (Figure S5A) further enhanced B-1a cell differentiation from WT versus *H2-M*$^{-/-}$ donors (Figures S5B and S5C),

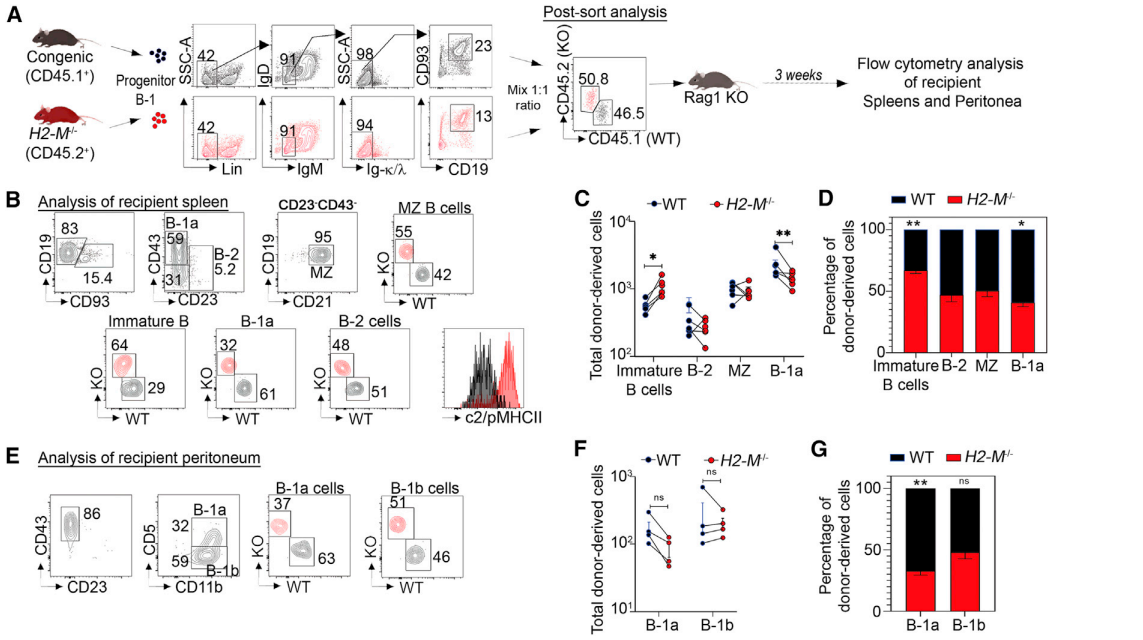

Figure 4. Absence of H2-M-MHCII interaction affects the maturation and maintenance of B-1a cells

(A–G) (A) B-1 cell precursors were FACS-sorted from one-week-old congenic B6 mice (CD45.1$^+$) and *H2-M*$^{-/-}$ mice (CD45.2$^+$), mixed in 1:1 ratio before adoptive transfer into *H2-M*$^{-/-}$ mice. The recipient Rag-deficient mice were sacrificed three weeks following the transfer; the spleen and peritoneal exudates were harvested and analyzed by flow cytometry. Gating strategy followed for FACS of B-1 cell precursors (Lin$^-$Ig$^-$CD19$^+$B220$^{lo/-}$CD93$^+$) from WT (CD45.1$^+$, black) and *H2-M*$^{-/-}$ mice (CD45.2$^+$, red). Post-sort analysis was shown to indicate ~95% purity. Gating strategy, scatterplot indicating the total cell number and the bar graph showing the percentage of donor-derived cells developed from sorted and transplanted B-1 cell precursors of WT congenic (black) and H2-M-deficient donor (red) mice recovered from the spleen (B, C, D) and peritoneum (E, F, G) of recipient *Rag1*$^{-/-}$ mice. Each point indicates an individual animal. *, $p < 0.05$, **, $p = 0.0043$ (multiple *t* test one per row). Each contour plot graph shows a maximum of 8,000 events. Data representative of two independent experiments with n = 4–5 mice/group. All the bar graphs or scatterplots are presented as mean ± SEM.

interaction of H2-M$^+$ B-1a precursors with CD4$^+$ T cells, via p/MHCII:TCR, may promote differentiation.

Absence of H2-M skews the B-1 immunoglobulin (Ig) repertoire

B-1a cells produce most of the natural IgM antibodies, including a germline-encoded repertoire. However, the reduced B-1 cell population in *H2-M*$^{-/-}$ mice resulted in only slightly lower IgM levels (Figure 5A). We saw no titer differences between WT and *H2-M*$^{-/-}$ mice for Abs to the B-1a specific antigens, PtC and PC, but observed a small, significant decrease in titers to nitrophenyl (NP) in *H2-M*$^{-/-}$ mice (Figure 5A). Moreover, NP-ficoll immunization induced a significant increase in NP-specific B-1a cells and IgM response in WT over *H2-M*$^{-/-}$ mice (Figures S5D–S5F). These results revealed bias in the selection of the B-1a cell IgM repertoire in the absence of H2-M.

To further investigate repertoire, we measured the frequency of B-1a PtC-specific cells in *H2-M*$^{-/-}$ mice, using fluorophore-conjugated PtC liposomes. Approximately 14% of *H2-M*$^{-/-}$ splenic B-1a cells expressed PtC-specific BCRs, compared with 8% in WT (Figures 5B and 5C); there was no strain difference in the absolute number of splenic PtC-specific B-1a cells (Figure 5C) and no clonal enrichment in *H2-O*$^{-/-}$ splenic B-1a cells (Figures S5G and S5H). In the peritoneum, 31% of *H2-M*$^{-/-}$ B-1a cells were PtC-specific, compared with 21% in WT (Figures 5D and 5E), with no difference in the absolute number of PtC-specific B-1a cells (Figure 5E). Splenic PtC-specific B-1a cells were enriched in *MHCII*$^{-/-}$ but not *MHCII*$^{+/-}$ mice (Figures S5G and S5H). Thus, loss of c1p/MHCII in *H2-M*$^{-/-}$ and *MHCII*$^{-/-}$ mice (Figure S3E), rather than reduced MHCII expression, appears responsible for the clonal bias in *H2-M*$^{-/-}$ B-1a cells. *H2-M*$^{-/-}$ B-1a cells also showed clonal enrichment for transcripts of quintessential B-1a IgH genes, including *Ighv11*, *Ighv12-03*, *Ighv6-06*, and *Ighv1-55* (Figure S5I). Importantly, PtC-specific B-1a cells were also enriched in H2-M$^{-/-}$ BALB/c (I-A^d) mice (Figure 5F), although in these mice, B-1a cell numbers were not detectably reduced (Figure 1M). These results reveal that H2-M absence influences PtC$^+$ B-1a clonal enrichment, independent of MHCII haplotype.

Based on these results, we hypothesized that lack of H2-M/MHCII interaction biases BCR-mediated B-1a selection during development. We found that, relative to WT mice, *H2-M*$^{-/-}$ mice had smaller clonal expansions or possibly lower expression levels of IgH transcripts per cell (Figure 5G). We then took the 50 clonotypes with the most reads from each mouse and investigated their relative contribution to the observed repertoire in that mouse (Figure 5H). *H2-M*$^{-/-}$ mice had less of their IgH repertoire accounted for by their 50 largest clonotypes,

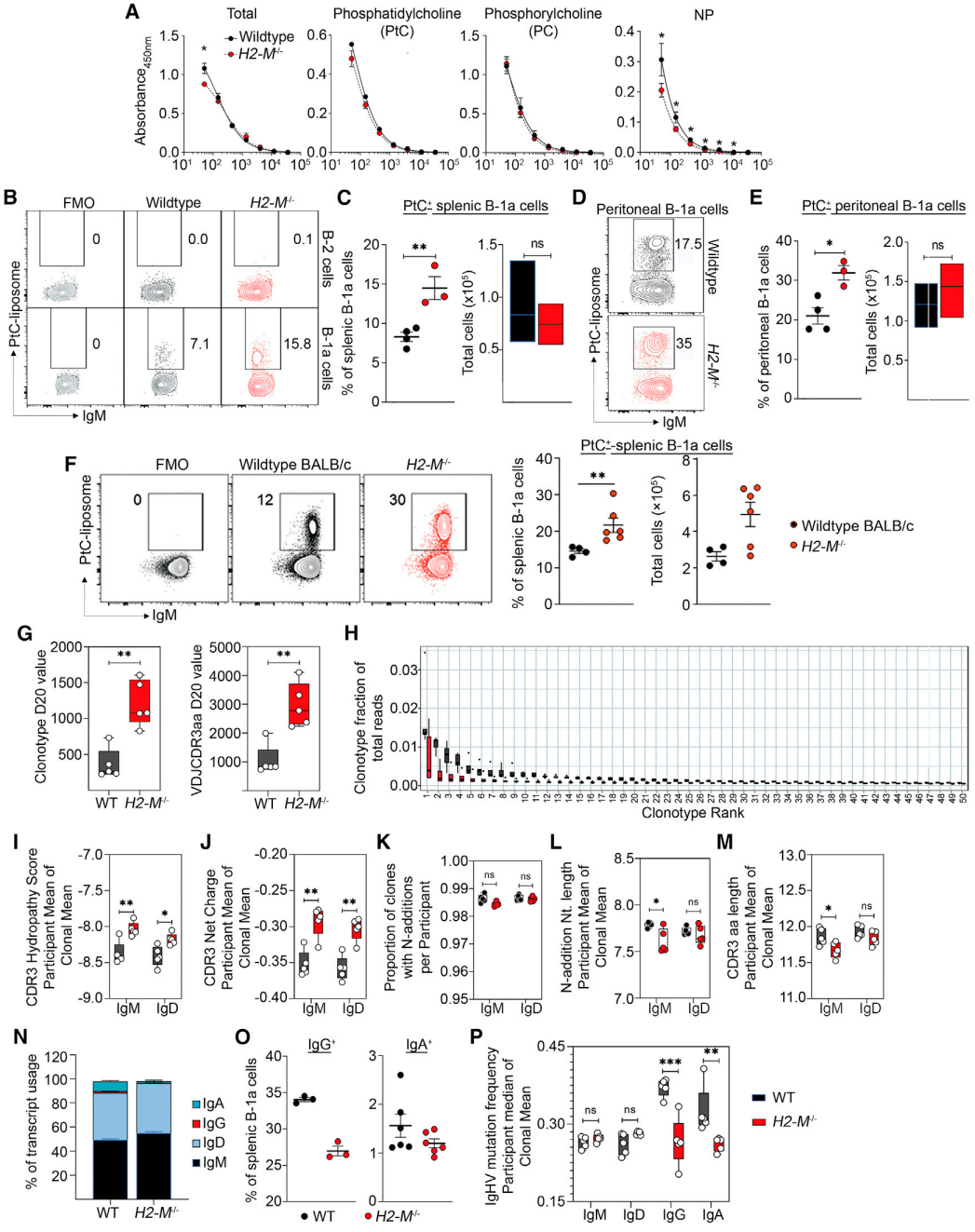

Figure 5. The absence of H2-M skews B-1 immunoglobulin specificities and IgH repertoires

(A) Serum IgM Ab titer measured by ELISA to indicate total IgM level and IgM level against PtC, PC, and 4-hydroxy-3-nitrophenylacetyl (NP) between WT (black) and *H2-M*$^{-/-}$ mice (red).

(B) Representative flow plots showing IgM expression and binding of PtC-liposome by B-1a cells from the spleens of WT and *H2-M*$^{-/-}$ mice. FMO control was shown to identify the positive binding of B-1a cells for PtC-liposome.

(C) Percentage and the total number of mature B-1a cells showing binding of PtC-liposome in the spleens of WT and *H2-M*$^{-/-}$ mice.

(D) Representative contour plots showing IgM expression and PtC-liposome binding by B-1a cells from the peritoneal cavity of WT and *H2-M*$^{-/-}$ mice.

(E) Percentage and the total number of mature B-1a cells showing binding of PtC-liposome from the peritoneum of WT and *H2-M*$^{-/-}$ mice.

(legend continued on next page)

consistent with the presence of smaller clones than WT or lower transcript expression per cell. Altogether, the repertoire analyses argue that H2-M absence affects clonal distribution of splenic B-1a cells and expands certain canonical B-1a specificities, such as PtC.

H2-M affects B-1 cell BCRs

We also assessed biochemical properties of B-1a CDR-H3 from WT and *H2-M*$^{-/-}$ mice. A significantly higher CDR-H3 hydropathy score and fewer negatively charged residues were observed for germline *H2-M*$^{-/-}$ B-1a-expressed IgM and IgD versus WT counterparts (Figures 5I and 5J). Although comparable proportions of B-1a cells showed N-junctional addition (Figure 5K), *H2-M*$^{-/-}$ B-1a cells had short N-additions, whereas WT B-1a cells had a small but significant increase in N-addition length (Figure 5L). This was reflected in a significant difference in the CDR-H3 length (germ-line segment-encoded + N nucleotides) (Figure 5M).

We also observed an H2-M effect on the frequency of class-switch recombination in B-1a cells. Compared with *H2-M*$^{-/-}$ splenic B-1a cells, WT B-1a cells had significantly higher proportions of class-switched transcripts (Figure 5N) and IgG^{+} B-1a cells (Figure 5O). WT peritoneal B-1 cells showed a significantly higher percentage of IgG^{+} and IgA^{+} B-1 cells (Figure S6A). Class-switched IgH (IgG and IgA) in *H2-M*$^{-/-}$ B-1a cells had a lower mutation frequency than in WT (Figure 5P). These results indicated that H2-M deficiency limits somatic hypermutation and class-switch recombination in mature B-1a cells, potentially restricting the selection and/or expansion of mature B-1a cell clones.

MHCII participates in the BCR signalosome in a cargo-dependent manner

MHCII shares overlapping signaling adapters (Ig-α/β) with the BCR (Lang et al., 2001). Hence, we hypothesized that the H2-M-mediated effects on B-1a cells were due to peptide cargo-dependent, MHCII contribution to BCR signaling. We first analyzed the MHCII localization relative to BCR on splenic B cells by immunofluorescence. In WT B cells, c1p/MHCII molecules generated punctate staining, a portion of which colocalized with BCR and with Ig β-chain, whereas c2p/MHCII did not (Figure 6A). In *H2-M*$^{-/-}$ B cells, which are enriched for surface c2p/MHCII, MHCII and BCR did not colocalize. Particularly in WT B cells, c1p/MHCII, but not c2p/MHCII, strongly colocalized with tetraspanin CD9, indicating preferential c1p/MHCII recruitment to the signalosome complex (Figure 6A). Notably, specifically in *H2-M*$^{-/-}$ B cells, c2p/MHCII showed a small but significant increase in co-localization with STING proteins, which dampen BCR signaling (Figure 6A) (Tang et al., 2021). To investigate proximity in the nanometer range, we used the proximity ligation assay (PLA), which confirmed proximity of c1p/MHCII, but not c2p/MHCII, to BCR (Figures 6B and 6C). Quantitatively, WT B cells had significantly higher IgM:c1p/MHCII PLA signals than *H2-M*$^{-/-}$ B cells but no difference in IgM:c2p/MHCII PLA signals, which were overall low (Figure 6C).

To help understand differences in the behavior of the c1p/MHCII and c2p/MHCII, and the effect of *H2-M* deficiency, we characterized eluted peptide cargo by mass spectrometry. Deficiency of the human H2-M ortholog, HLA-DM, is associated with MHCII presentation of peptides with lower MHCII affinity (Alvaro-Benito et al., 2018), as it has not been evaluated in mice, but the MHCII peptidome in *H2-O*$^{-/-}$ mice (high DM activity) has increased MHCII affinity (Nanaware et al., 2019). To directly assess the effect of *H2-M* deficiency in murine B cells, we isolated total I-A^{b} from *H2-M*$^{-/-}$ splenic B cells and analyzed bound peptides (Table S1). By comparison with published peptidomes from WT B6 mice (Clement et al., 2021; Nanaware et al., 2021), *H2-M* deficiency causes a shift in the distribution of predicted peptide-MHCII affinity to lower values (Figure 6D). As in previous studies (Alvaro-Benito et al., 2018; Nanaware et al., 2019), these affinity changes are not accompanied by alterations in the length distribution or intracellular sources of peptide cargo (Table S1). We extended these studies to the c1p/MHCII and c2p/MHCII subsets of the total I-A^{b} peptidome. Although fewer peptides were available for analyses, a clear reduction in affinity for c2p/MHCII cargo relative to c1p/MHCII is observed (Figure 6D), again with comparable peptide lengths or intracellular sources (Table S1, Figure S6A). c1p/MHCII, but not c2p/MHCII conformer, showed expected preferred binding patterns of large hydrophobic residue at the P1 and small hydrophobic residues (preferentially Proline) at P4 and P6 positions (Figure S6B). Thus, the co-localization of c1p/MHCII, but not c2p/MHCII, with BCR is associated with higher-affinity peptide cargo.

BCR-mediated signaling is attenuated in *H2-M*$^{-/-}$ B-1 cells

To analyze BCR-mediated signaling in mature B-1 cells, we measured phosphorylated Btk (pBtk) as an upstream BCR signaling event and Nur77, a distal downstream reporter (Huizar et al., 2017). Splenic B-1a cells showed significantly higher Nur77 levels than FO and MZ B cells (Figures S6B and S6C), irrespective of total surface Ig (Figure S6D). pBtk and Nur77 levels

(F) Representative contour plots showing IgM expression and PtC-binding by splenic B-1a cells from WT and *H2-M*$^{-/-}$ mice of BALB/c background and the corresponding quantification. FMO indicates fluorescent-minus-one control.
(G and H) (G) D20 metric analysis quantifying clonal variation and IgH CDR3 diversity and (H) clonotype rank analysis for mature splenic B-1a cell subset from week six old WT (black) and *H2-M*$^{-/-}$ (red) mice.
(I and J) (I) The hydropathy score and (J) CDR3 net charge of IgH sequences obtained from unmutated splenic B-1a cells of WT (black) and *H2-M*$^{-/-}$ mice (red), separated according to their isotype sub-classes.
(K–M) (K) Percentages of IgH sequences containing N-nucleotide insertions at CDR3 junctions from splenic B-1a cells. Bar graph indicating (L) the length of N-nucleotide additions at IgH CDR3 junctions and (M) the length of IgH CDR3 sequences of unmutated splenic B-1a cells obtained from WT and *H2-M*$^{-/-}$ mice.
(N) Stacked bar graph showing frequencies of each distinct isotype sequences from WT and *H2-M*$^{-/-}$ mice, IgG = (IgG1+IgG2a + IgG2b + IgG2c + IgG3).
(O) Percentage of splenic B-1a cells showing expression of IgG and IgA by flow cytometry analysis of WT (black) and *H2-M*$^{-/-}$ (red) mice.
(P) The frequencies of mutated sequences from splenic B-1a cells of WT and *H2-M*$^{-/-}$ mice, presented according to their isotype sub-class sequences. Data representative of three (A–E) or one (F–P) independent experiments with n = 3–5 mice/group. All the scatterplots are presented as mean ± SEM.

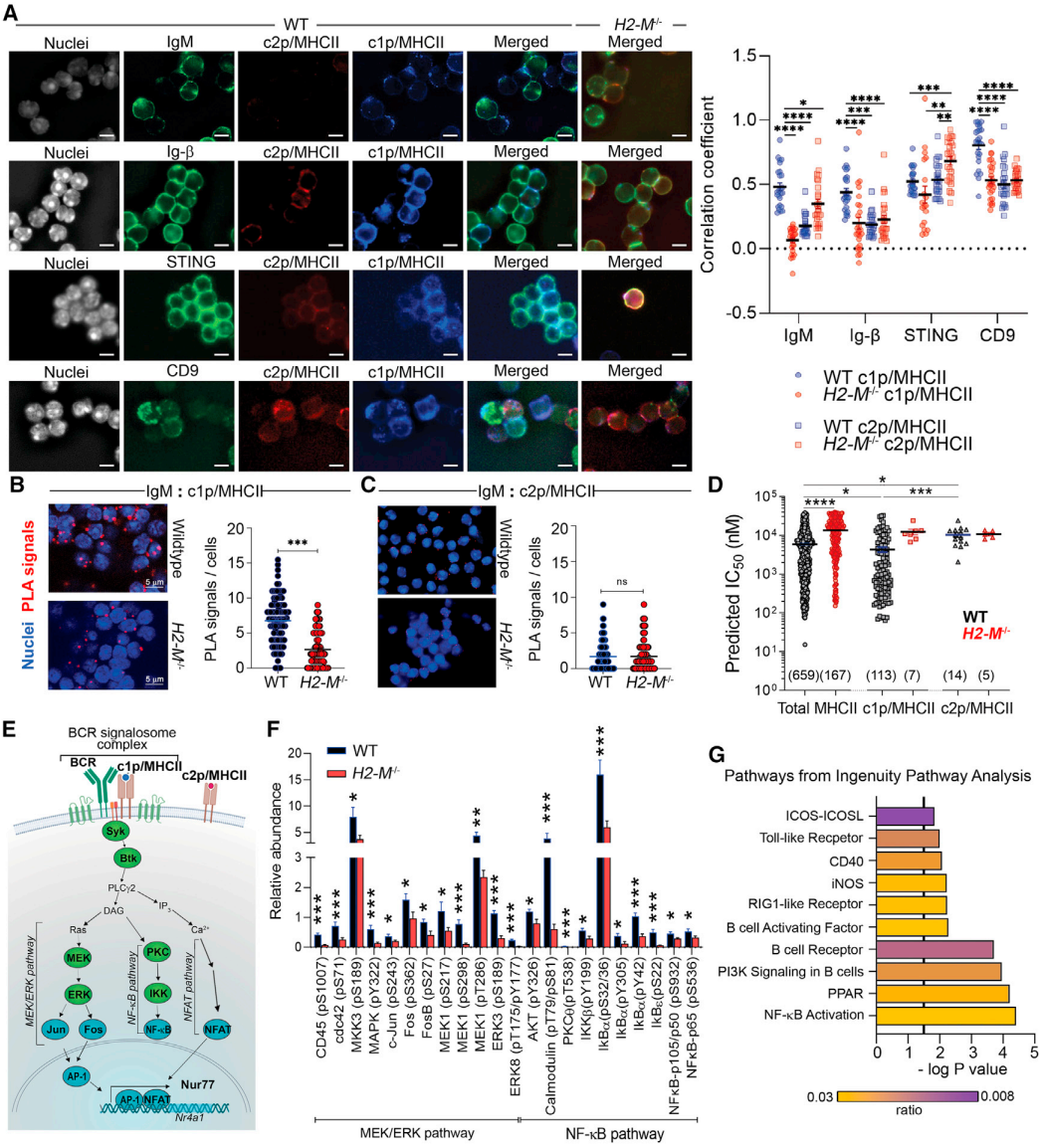

Figure 6. The absence of H2-M downregulates BCR signaling

(A–C) (A) Representative immunofluorescence images showing surface expression of IgM, Ig-β, tetraspanin protein CD9, c1p/MHCII, and c2p/MHCII and intracellular STING expression by B cells from WT and *H2-M*$^{-/-}$ mice. Scale bar represents 5 μm length. Scatterplots show the corresponding correlation coefficient between c1p/MHCII (circle) and c2p/MHCII (square) with surface IgM, Ig-β, CD9 (Won and Kearney, 2002), or intracellular STING expressions from B cells derived from WT (blue) and *H2-M*$^{-/-}$ (red) mice. Splenic B cells from WT and *H2-M*$^{-/-}$ mice were fixed with 2% paraformaldehyde for 30 min, and PLA was performed. Representative images of PLA (red dots) and quantification of PLA images are shown for IgM:c1p/MHCII (B) and IgM:c2p/MHCII (C) PLA studies. Scale bar, 25 μm. For extended images with a higher magnification, scale bar represents 5 μm. ***, $p < 0.0001$ (Mann-Whitney U test).

(D) The NetMHCII pan 3.2 predicted binding affinity for the I-A^{b} peptides using M5/114 (total MHCII, circle), KH74 (c1p/MHCII, square), and 15G4 (c2p/MHCII, triangle) antibody eluted from WT (black) and H2-M$^{-/-}$ (red) C57BL/6 mice with length ≥ 12 amino acids are plotted. The significant differences are indicated, and the numbers of peptides in each set are indicated on the plot.

(E) Schematic showing key components of BCR signaling pathway. BCR forms interacts with signal-transducing Ig-α/β, c1p/MHCII, and tetraspanin proteins (CD9) to form signalosome complex on B cell surface. Green and blue symbols indicate involved key kinases and transcription factors, respectively.

(F) Bar graph analysis of the relative expression of a subset of signaling proteins in the BCR signaling pathway in B-1 cell precursors from WT (black) over *H2-M*$^{-/-}$ (red) mice.

(G) The top ten pathways by IPA analysis in WT versus *H2-M*$^{-/-}$ B-1 cell precursors. Data representative of two independent (A–C) or one (E–G) experiment with n = 3–4 mice/group. All the bar graphs or scatterplots are presented as mean ± SEM.

were higher in WT versus *H2-M*$^{-/-}$ splenic B-1 cells (Figure S6E), whereas levels of IgM or CD5, an inhibitor of BCR-mediated signaling (Gary-Gouy et al., 2002), did not differ, consistent with the effects being due to H2-M deficiency (Figure S7E).

Given the critical role of BCR signaling for B-1a development and our results on B-1 differentiation (above), we hypothesized that c1p/MHCII in B-1 precursors provide survival and differentiation signals through an Ig-α/β-mediated contribution to integrated BCR signaling. (A schematic of relevant BCR signaling pathways is shown in Figure 6E). No difference in intracellular levels of Ig-α/β was detected in WT versus *H2-M*$^{-/-}$ B-1 precursors, but WT precursors had higher expression of pBtk (Figure S7F). To obtain a broader view of BCR signaling, we used an immune-receptor phospho-array. Compared with *H2-M*$^{-/-}$ B-1 precursors, WT had significantly higher levels of activated BCR signaling pathway proteins (Figures S7G and S7H); this was particularly notable for the MEK/ERK and NF-κB signaling cascades (Figure 6F). Analysis of differentially activated proteins identified signatures in pathways associated with co-stimulatory B cell activation (Figure 6G).

In a direct stimulation assay using anti-total MHCII Ab, the formation of IgM/p/MHCII complexes (PLA signals, red dots) (Figures 7A and 7B) and their co-localization with Ig-β protein (yellow signals) (Figure 7A) were significantly increased in WT but not *H2-M*$^{-/-}$ B-1a cells. MHCII-mediated stimulation also induced significantly higher levels of pBtk and Nur77 (but not pAkt) over time in WT versus *H2-M*$^{-/-}$ mature B-1a cells (Figures 7C and 7D) as well as higher pSyk, pBtk, and total IκBa levels (Figures 7E and 7F). In contrast, stimulation with a monoclonal α-Ig-κ antibody did not induce substantial (prolonged) differences in BCR signaling proteins pBtk, pAkt, or Nur77 (Figure S8A). Thus, in mature B-1 cells, MHCII ligation leads to co-stimulatory signaling, likely through a c1p/MHCII-IgM-Ig-α/β complex, to contribute to the integrated BCR signaling pathway. However, in the absence of H2-M, this co-stimulatory signal is dampened, likely through suboptimal assembly of this tertiary complex. Consistent with this, c1p/MHCII stimulation in mature WT B-1 cells increased pBtk and Nur77, whereas c2p/MHCII stimulation in *H2-M*$^{-/-}$ B-1 cells increased STING activation (Figure S8B). Overall, H2-M deficiency resulted in reduced BCR-associated signaling in B-1 cells.

DISCUSSION

To assess the effects of H2-M on B-1a cells, we studied *H2-M*$^{-/-}$ mice on the C57BL/6 background, which express a single MHCII allele, I-A^b. I-A^b has a high affinity for CLIP peptide and requires H2-M for peptide exchange (Cresswell, 1996). The B6 model offered a reductionist system to study H2-M effects on B-1a development and repertoire. Of note, high CLIP affinity and H2-M (or DM) dependence for peptide exchange is shared by many common human and mouse MHC-II proteins (Kropshofer et al., 1999), suggesting that paradigms discovered here are likely relevant in other MHCII contexts. Indeed, we have been able to replicate some key findings in other genotypes, as discussed below.

A key finding in the H2-M-knockout model was a cell-intrinsic effect on B-1 cell development (the biased CD4$^+$ T cell repertoire also may contribute). The expression of I-A^b proteins with altered peptide cargo and conformation (c2p/MHCII conformers) was linked to reduced B-1 self-renewal and survival and diminished B-1a cell numbers. H-2M$^{-/-}$ mice also harbored an altered B-1a Ig repertoire that favored BCR recognizing highly abundant antigens. Our signaling studies in B6 *H2-M*$^{-/-}$ B-1 cells showed reduced activation of MHCII-mediated co-stimulatory pathways that contribute to an integrated BCR signal. This signaling defect likely underlies the similarly skewed B-1a Ig repertoire BALB/c *H2-M*$^{-/-}$ mice. The apparent basis of altered signaling was the exclusion of c2p/MHCII conformers of I-A^b from BCR-signalosome-containing microdomain. We also have observed selective, conformation-based recruitment to the BCR signalosome in human T2.DR3.DM versus T2.DR3 cells. DM-resistant, peptide-bound DR3 molecules showed proximity to surface BCR, whereas CLIP-DR3 complex did not (Figures S9A and S9B). Altogether, these findings argue for a generalizable effect of peptide cargo on MHCII association with BCR signalosome and co-stimulatory signaling, with a striking impact on B-1a cells in mice. For human MHCII, DM-sensitive peptide cargo has been associated with distinct conformational alterations and dynamic flexibility throughout the MHCII molecule (Reyes-Vargas et al., 2020; Yin et al., 2014). It is possible that interactions with BCR, Ig-$\alpha/$Ig-β, or other signalosome components are sensitive to similar alterations.

Reduced BCR signaling in the absence of H2-M could be the primary reason for the limited self-renewal ability of mature B-1a cells, as BCR signal strength regulates this capacity (Nguyen et al., 2017). BCR-mediated signals integrate with signals from positive and negative co-stimulators, with the net effect influencing B cell fate (reviewed in Baumgarth, 2017). Strong overall BCR signaling is critical for the selection and maintenance of the B-1a cell population (Nguyen et al., 2017; Zhou et al., 2015). Our findings corroborate prior evidence demonstrating the effect of positive BCR co-receptor signaling on B-1a cell survival. Notably, however, our data specifically highlight the influence of MHCII signaling on the selection and maintenance of B-1a cells and also show the critical role of H2-M as a BCR signal modulator. Several other models, where BCR-signal regulatory proteins such as CD5 (Bikah et al., 1996) and CD6 (Enyindah-Asonye et al., 2017) are deleted, showed reduced B-1a cell maturation. However, these proteins are rarely lost physiologically. In contrast, there are natural alleles of MHCII and HLA-DM that affect their interaction and alter levels of edited p/MHCII. These alleles would be predicted to modulate BCR signal strength with consequences for abundance and repertoire selection of human B cells selected by activation of BCR signalosome.

We also found that absence of H2-M yields B-1a cell clonotypes with smaller expansions or lower IgH transcript expression in the spleen. Mature B-1a cells in *H2-M*$^{-/-}$ mice have reduced self-renewal ability and increased apoptosis, likely reducing clonal sizes. Abrogated BCR signaling likely underlies these phenotypes. Notably, despite missing an H2-M/MHCII-mediated secondary signal, PtC-specific B-1a cells develop and expand prominently to occupy a significant proportion of splenic B-1a cells in *H2-M*$^{-/-}$ mice. PtC is the most abundant phospholipid antigen, implying that if the cognate antigen is accessible and

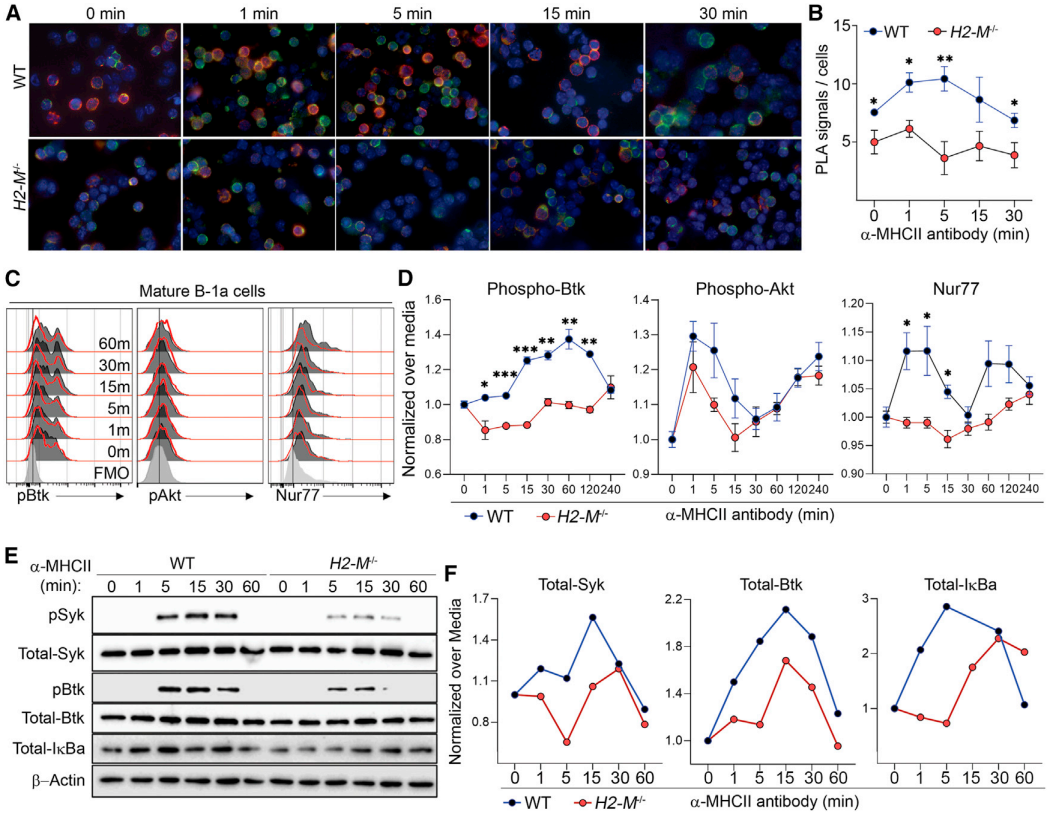

Figure 7. MHCII-mediated stimulation preferentially activates the BCR signaling in mature B-1a cells from WT compared with *H2-M*$^{-/-}$ mice

Mature B-1a cells (CD19^{+}B220$^{lo/-}$CD93^{-}CD43^{+}CD5^{+}CD23^{-}) were FACS-sorted from the spleens of WT (black) and *H2-M*$^{-/-}$ mice (red). The cells were cultured *in vitro* in the presence or absence of anti-total MHCII antibody for the indicated duration to determine the BCR signaling events (pBtk, pAkt, and Nur77). Activation of the cells was assessed by intracellular staining of pAkt, pBtk, and Nur77 in mature B-1a cells. (A) Representative immunofluorescence images showing the IgM:c1p/MHCII PLA signals (red dots) and the intracellular expression of Ig-β (green) by mature B-1 cells from WT and *H2-M*$^{-/-}$ mice following treatment with anti-MHCII antibody for 0, 1, 5, 15, and 30 min; nuclei are shown with DAPI staining (blue).

(B) Quantification of the PLA images (A) are shown for IgM:p/MHCII PLA studies with mature B-1 cells from WT (Black dots) and *H2-M*$^{-/-}$ mice (red dots).

(C) Representative histograms indicated the expression level of pBtk, pAkt, and Nur77 by mature B-1a cells from WT (shaded black) and *H2-M*$^{-/-}$ (red line) at various time durations indicated. Gray-filled histogram indicating corresponding FMO controls.

(D) Dot plots indicated the relative abundance of the BCR signal events in mature B-1a cells from WT (black dots) and *H2-M*$^{-/-}$ (red dots) mice. Relative abundance for protein was measured by dividing MFI for the protein in the presence of a stimulant over the MFI for the corresponding protein obtained from a culture of the cells with media alone. *, $p < 0.05$, **, $p < 0.01$, ***, $p < 0.005$ (*t* test). Data are representative of two independent experiments.

(E) Magnetic bead-purified mature B-1 cells from the spleens of WT and *H2-M*$^{-/-}$ mice were stimulated with anti-MHCII antibody for indicated time spans, harvested, and examined by Western blot. Data are from one representative experiment of two independent experiments.

(F) Quantitation of Western blot data in (E). Signal was normalized to beta-actin and further normalized to mature B-1 cells at time 0, giving a value of 1. Data representative of one (A–B, E–F) or two (C-D) independent experiments with n = 3–4 mice/group. All the scatterplots are presented as mean ± SEM.

abundant, the requirement for an H2-M/MHCII-derived signal is dispensable for B-1a survival and maintenance. Thus, our results argue that H2-M-dependent MHCII-mediated signaling acts as a co-stimulator and is essential for selection of B-1a cells specific for less abundant antigens.

Several recent studies emphasize the importance of somatic hypermutation, N-junctional addition, and class-switch recombination in the maturation of the B-1a immunoglobulin repertoire (Yang et al., 2015). For B-1a cells, the accumulation of somatic mutations occurs in an age-dependent manner driven by endogenous antigens (Reynaud et al., 1995). We found that N-junctional insertions and somatic hypermutation were significantly reduced in the absence of H2-M, particularly in the class-switched B-1a cells. The first wave of murine B-1a development during fetal and neonatal life (until postnatal day 4) occurs in the absence of TdT, resulting in a BCR repertoire that lacks N-insertion. The second wave of murine B-1a cell development occurs during neonatal life when B-1a cells acquire TdT expression for N-junctional insertions. Lack of H2-M did not reduce the most abundant PtC-specific B-1a cell population, which was found in significantly higher frequency in *H2-M*$^{-/-}$ versus WT mice. PtC, a quintessential B-1a cell specificity that uses V_H11 and V_H12 genes, also shows minimal usage of N-junctional insertion and somatic hypermutation (Feeney, 1990; Wang and Clarke,

2004; Yang et al., 2015). This result argues that H2-M-selected p/MHCII signaling directly influences the second wave of B-1a development (TdT-dependent). A similar distribution of less expanded, more diverse polyclonal B-1-like cells can be observed in young versus older humans (Rodriguez-Zhurbenko et al., 2019). With advancing age, the B-1 cell population becomes less diverse, with more oligoclonal expansions. Our results suggest that the efficient maturation and expansion of these TdT-dependent B-1a cells could rely on signaling by the H2-M-selected p/MHCII complexes.

An interesting question is whether there is a requirement for an MHCII ligand for the B-1 cell maturation pathway. B-1 cells are found to associate with follicular dendritic cells and expand at the center of the B cell follicles in the spleen (Wen et al., 2005). Immature and mature B-1 cells show the highest expression of CXCR5 within splenic B cell subsets (Ansel et al., 2002; Wen et al., 2005), the receptor for chemokine CXCL13, which directs their migration efficiently to the center of B cell follicles. It remains to be determined whether T follicular helper (Tfh) cells at this site provide maturation signals for further selection and survival of B-1 cells. Our experiment with co-transfer of $CD4^+$ T cells suggests that T cells enhance B-1 cell differentiation.

Antiphospholipid syndrome (APS) is characterized by persistent elevation of antiphospholipid antibodies (aPL), the antibody class elevated in *H2-M*$^{-/-}$ mice. Interestingly, HLA-DMA allelic variations are linked to APS (Sanchez et al., 2004), raising the possibility that reduced DM function contributes to aPL generation by influencing the Ab repertoire through mechanisms such as those we report here. Our findings also raise the possibility of DM effects on host defense and autoimmunity through alterations in the development and selection of polyreactive B-1 cells or cells with similar functions in humans (Chen et al., 2020).

Our study links the regulation of peptide occupancy of MHCII to early development of an APC lineage. For B-1 cells, this is mainly due to H2-M/MHCII-mediated regulation of BCR signaling and its downstream effects. However, the expression of non-classical MHCII proteins may have regulatory effects on the development of other APCs. For example, H2-M deficiency significantly boosted the abundance of MZ B cells in B6 mice (Figures 1J and 1K), an effect that was not pursued here due to lower dependency of MZ B cell development on BCR signaling. Further studies of possible developmental regulation of APC lineages by non-classical MHCII proteins are warranted.

Limitations of the study

We studied the effects of H2-M function on BCR signaling and B-1a cell development primarily using the C57BL/6 mouse strain, although the key finding of repertoire bias was also observed in BALB/c mice. It remains possible that different effects on BCR signaling and consequent cell numbers or Ig repertoire will differ in different strains. This strain dependence would be based on the degree of interaction of H2-M and the MHCII alleles expressed, which varies allelically for both H2-M and MHCII proteins with consequences for peptide editing (Alvaro-Benito et al., 2015; Zhou et al., 2017). Another limitation is related to mouse/human differences as regards B-1 cells. B-1 cells are well studied in mice, but a simple human counterpart has not been identified, and current investigations seek cells with homologous phenotypes and functions. Consequently, we could only speculate regarding a possible impact of HLA-DM on phospholipid-specific, B-1-like innate cells in humans. Third, in the absence of a cell-specific H2-M knockout model, the maximal functional impact of H2-M deficiency in B cells (particularly B-1 cells) on subsequent interactions with other immune cells, on T cell selection, and on B-1 cell-dependent immune reactions in autoimmune models is unknown and remains to be studied.

STAR★METHODS

Detailed methods are provided in the online version of this paper and include the following:

- KEY RESOURCES TABLE
- RESOURCE AVAILABILITY
  - Lead contact
  - Materials availability
  - Data and code availability
- EXPERIMENTAL MODEL AND SUBJECT DETAILS
  - Mice
  - Cell lines
- METHOD DETAILS
  - Flow cytometry
  - Cell isolation
  - RNA extraction and qPCR
  - Immunofluorescence
  - ELISA
  - *In vivo* adoptive cell transfer
  - BrdU incorporation analysis
  - *In vitro* stimulation and cell culture
  - Immunoglobulin repertoire analysis
  - Proximity ligation assay
  - Immunoblot analysis
  - Immunopeptidome analysis
- QUANTIFICATION AND STATISTICAL ANALYSIS

SUPPLEMENTAL INFORMATION

Supplemental information can be found online at https://doi.org/10.1016/j.celrep.2021.110200.

ACKNOWLEDGMENTS

We thank Dr. Nicole Baumgarth for critical review and helpful discussion of the manuscript. We thank Dr. Lisa Denzin for providing the anti-mouse H2-O (Mags.Ob1) conjugated with AF647 (Fallas et al., 2007) and the cell lines T2.DR3 and T2.DR3.DM. Cell sorting/flow cytometry analysis for this project was done on instruments in the Stanford Shared FACS Facility (grant support: S10RR027431-01 for LSRII.UV). Microscopy images were acquired using the Zeiss AxioImager Epifluorescence/Widefield Microscope in the Cell Sciences Imaging Facility, Stanford. Phospho-array data were acquired with the help of the Stanford Functional Genomics Facility. This work was supported by the Stanford Maternal and Child Health Research Institute (MCHRI) (DG), the Daylight Foundation, the Gupta Foundation, Lucile Packard Foundation for Children's Health (EDM), and Lowance Center for Human Immunology (EEBG).

AUTHOR CONTRIBUTIONS

Conceptualization, D.G., L.N.A., and E.D.M.; methodology, D.G., T.D.P., X.H., P.P.N., D.S., C.G.L., M.E.M., and K.D.N.; software, D.G., T.D.M., and P.P.N.;

investigation, D.G., T.D.P., and S.D.B., resources, A.B.K., D.S., L.C.E., and P.E.J.; writing—original manuscript, D.G.; review and editing, L.A.H., L.J.S., S.D.B., E.E.B.G., and E.D.M.; supervision, L.A.H., E.E.B.G., S.D.B., and E.D.M.

DECLARATION OF INTERESTS

The authors declare no competing financial interest.

Received: October 19, 2020
Revised: September 23, 2021
Accepted: December 13, 2021
Published: January 25, 2022

REFERENCES

Alvaro-Benito, M., Wieczorek, M., Sticht, J., Kipar, C., and Freund, C. (2015). HLA-DMA polymorphisms differentially affect MHC class II peptide loading. J. Immunol. *194*, 803–816.

Alvaro-Benito, M., Morrison, E., Abualrous, E.T., Kuropka, B., and Freund, C. (2018). Quantification of HLA-DM-dependent major histocompatibility complex of class II immunopeptidomes by the peptide landscape antigenic epitope alignment utility. Front. Immunol. *9*, 872.

Andreatta, M., Lund, O., and Nielsen, M. (2013). Simultaneous alignment and clustering of peptide data using a Gibbs sampling approach. Bioinformatics *29*, 8–14.

Ansel, K.M., Harris, R.B., and Cyster, J.G. (2002). CXCL13 is required for B1 cell homing, natural antibody production, and body cavity immunity. Immunity *16*, 67–76.

Baumgarth, N. (2011). The double life of a B-1 cell: self-reactivity selects for protective effector functions. Nat. Rev. Immunol. *11*, 34–46.

Baumgarth, N. (2017). A hard(y) look at B-1 cell development and function. J. Immunol. *199*, 3387–3394.

Bikah, G., Carey, J., Ciallella, J.R., Tarakhovsky, A., and Bondada, S. (1996). CD5-mediated negative regulation of antigen receptor-induced growth signals in B-1 B cells. Science *274*, 1906–1909.

Casola, S., Otipoby, K.L., Alimzhanov, M., Humme, S., Uyttersprot, N., Kutok, J.L., Carroll, M.C., and Rajewsky, K. (2004). B cell receptor signal strength determines B cell fate. Nat. Immunol. *5*, 317–327.

Chan, V.W., Meng, F., Soriano, P., DeFranco, A.L., and Lowell, C.A. (1997). Characterization of the B lymphocyte populations in Lyn-deficient mice and the role of Lyn in signal initiation and down-regulation. Immunity *7*, 69–81.

Chen, J.W., Rice, T.A., Bannock, J.M., Bielecka, A.A., Strauss, J.D., Catanzaro, J.R., Wang, H., Menard, L.C., Anolik, J.H., Palm, N.W., et al. (2020). Autoreactivity in naive human fetal B cells is associated with commensal bacteria recognition. Science *369*, 320–325.

Clement, C.C., Nanaware, P.P., Yamazaki, T., Negroni, M.P., Ramesh, K., Morozova, K., Thangaswamy, S., Graves, A., Kim, H.J., Li, T.W., et al. (2021). Pleiotropic consequences of metabolic stress for the major histocompatibility complex class II molecule antigen processing and presentation machinery. Immunity *54*, 721–736 e710.

Cox, J., and Mann, M. (2008). MaxQuant enables high peptide identification rates, individualized p.p.b.-range mass accuracies and proteome-wide protein quantification. Nat. Biotechnol. *26*, 1367–1372.

Cresswell, P. (1996). Invariant chain structure and MHC class II function. Cell *84*, 505–507.

Denzin, L.K., and Cresswell, P. (1995). HLA-DM induces CLIP dissociation from MHC class II alpha beta dimers and facilitates peptide loading. Cell *82*, 155–165.

Denzin, L.K., Robbins, N.F., Carboy-Newcomb, C., and Cresswell, P. (1994). Assembly and intracellular transport of HLA-DM and correction of the class II antigen-processing defect in T2 cells. Immunity *1*, 595–606.

Doebele, R.C., Pashine, A., Liu, W., Zaller, D.M., Belmares, M., Busch, R., and Mellins, E.D. (2003). Point mutations in or near the antigen-binding groove of HLA-DR3 implicate class II-associated invariant chain peptide affinity as a constraint on MHC class II polymorphism. J. Immunol. *170*, 4683–4692.

Enyindah-Asonye, G., Li, Y., Xin, W., Singer, N.G., Gupta, N., Fung, J., and Lin, F. (2017). CD6 receptor regulates intestinal ischemia/reperfusion-induced injury by modulating natural IgM-producing B1a cell self-renewal. J. Biol. Chem. *292*, 661–671.

Esplin, B.L., Welner, R.S., Zhang, Q., Borghesi, L.A., and Kincade, P.W. (2009). A differentiation pathway for B1 cells in adult bone marrow. Proc. Natl. Acad. Sci. U S A *106*, 5773–5778.

Fallang, L.E., Roh, S., Holm, A., Bergseng, E., Yoon, T., Fleckenstein, B., Bandyopadhyay, A., Mellins, E.D., and Sollid, L.M. (2008). Complexes of two cohorts of CLIP peptides and HLA-DQ2 of the autoimmune DR3-DQ2 haplotype are poor substrates for HLA-DM. J. Immunol. *181*, 5451–5461.

Fallas, J.L., Yi, W., Draghi, N.A., O'Rourke, H.M., and Denzin, L.K. (2007). Expression patterns of H2-O in mouse B cells and dendritic cells correlate with cell function. J. Immunol. *178*, 1488–1497.

Feeney, A.J. (1990). Lack of N regions in fetal and neonatal mouse immunoglobulin V-D-J junctional sequences. J. Exp. Med. *172*, 1377–1390.

Forster, I., and Rajewsky, K. (1987). Expansion and functional activity of Ly-1+ B cells upon transfer of peritoneal cells into allotype-congenic, newborn mice. Eur. J. Immunol. *17*, 521–528.

Gary-Gouy, H., Harriague, J., Dalloul, A., Donnadieu, E., and Bismuth, G. (2002). CD5-negative regulation of B cell receptor signaling pathways originates from tyrosine residue Y429 outside an immunoreceptor tyrosine-based inhibitory motif. J. Immunol. *168*, 232–239.

Ghosn, E.E., Sadate-Ngatchou, P., Yang, Y., Herzenberg, L.A., and Herzenberg, L.A. (2011). Distinct progenitors for B-1 and B-2 cells are present in adult mouse spleen. Proc. Natl. Acad. Sci. U S A *108*, 2879–2884.

Ghosn, E., Yoshimoto, M., Nakauchi, H., Weissman, I.L., and Herzenberg, L.A. (2019). Hematopoietic stem cell-independent hematopoiesis and the origins of innate-like B lymphocytes. Development *146*, dev170571.

Giudicelli, V., Chaume, D., and Lefranc, M.P. (2005). IMGT/GENE-DB: a comprehensive database for human and mouse immunoglobulin and T cell receptor genes. Nucleic Acids Res. *33*, D256–D261.

Gorga, J.C., Horejsi, V., Johnson, D.R., Raghupathy, R., and Strominger, J.L. (1987). Purification and characterization of class II histocompatibility antigens from a homozygous human B cell line. J. Biol. Chem. *262*, 16087–16094.

Gronwall, C., Vas, J., and Silverman, G.J. (2012). Protective roles of natural IgM antibodies. Front. Immunol. *3*, 66.

Guce, A.I., Mortimer, S.E., Yoon, T., Painter, C.A., Jiang, W., Mellins, E.D., and Stern, L.J. (2013). HLA-DO acts as a substrate mimic to inhibit HLA-DM by a competitive mechanism. Nat. Struct. Mol. Biol. *20*, 90–98.

Hardy, R.R., and Hayakawa, K. (2001). B cell development pathways. Annu. Rev. Immunol. *19*, 595–621.

Hayakawa, K., Tarlinton, D., and Hardy, R.R. (1994). Absence of MHC class II expression distinguishes fetal from adult B lymphopoiesis in mice. J. Immunol. *152*, 4801–4807.

Hayakawa, K., Asano, M., Shinton, S.A., Gui, M., Allman, D., Stewart, C.L., Silver, J., and Hardy, R.R. (1999). Positive selection of natural autoreactive B cells. Science *285*, 113–116.

Huizar, J., Tan, C., Noviski, M., Mueller, J.L., and Zikherman, J. (2017). Nur77 is upregulated in B-1a cells by chronic self-antigen stimulation and limits generation of natural IgM plasma cells. Immunohorizons *1*, 188–197.

Ishido, S., and Kajikawa, M. (2019). MHC class II fine tuning by ubiquitination: lesson from MARCHs. Immunogenetics *71*, 197–201.

Khan, W.N., Alt, F.W., Gerstein, R.M., Malynn, B.A., Larsson, I., Rathbun, G., Davidson, L., Muller, S., Kantor, A.B., Herzenberg, L.A., et al. (1995). Defective B cell development and function in Btk-deficient mice. Immunity *3*, 283–299.

Kobayashi, M., Lin, Y., Mishra, A., Shelly, C., Gao, R., Reeh, C.W., Wang, P.Z., Xi, R., Liu, Y., Wenzel, P., et al. (2020). Bmi1 maintains the self-renewal property of innate-like B lymphocytes. J. Immunol. *204*, 3262–3272.

Kropshofer, H., Arndt, S.O., Moldenhauer, G., Hammerling, G.J., and Vogt, A.B. (1997). HLA-DM acts as a molecular chaperone and rescues empty HLA-DR molecules at lysosomal pH. Immunity *6*, 293–302.

Kropshofer, H., Hammerling, G.J., and Vogt, A.B. (1999). The impact of the non-classical MHC proteins HLA-DM and HLA-DO on loading of MHC class II molecules. Immunol. Rev. *172*, 267–278.

Lang, P., Stolpa, J.C., Freiberg, B.A., Crawford, F., Kappler, J., Kupfer, A., and Cambier, J.C. (2001). TCR-induced transmembrane signaling by peptide/MHC class II via associated Ig-alpha/beta dimers. Science *291*, 1537–1540.

Liljedahl, M., Winqvist, O., Surh, C.D., Wong, P., Ngo, K., Teyton, L., Peterson, P.A., Brunmark, A., Rudensky, A.Y., Fung-Leung, W.P., et al. (1998). Altered antigen presentation in mice lacking H2-O. Immunity *8*, 233–243.

Montecino-Rodriguez, E., Leathers, H., and Dorshkind, K. (2006). Identification of a B-1 B cell-specified progenitor. Nat. Immunol. *7*, 293–301.

Montecino-Rodriguez, E., Fice, M., Casero, D., Berent-Maoz, B., Barber, C.L., and Dorshkind, K. (2016). Distinct genetic networks orchestrate the emergence of specific waves of fetal and adult B-1 and B-2 development. Immunity *45*, 527–539.

Morcos, M.N.F., Schoedel, K.B., Hoppe, A., Behrendt, R., Basak, O., Clevers, H.C., Roers, A., and Gerbaulet, A. (2017). SCA-1 expression level identifies quiescent hematopoietic stem and progenitor cells. Stem Cell Rep. *8*, 1472–1478.

Nanaware, P.P., Jurewicz, M.M., Leszyk, J.D., Shaffer, S.A., and Stern, L.J. (2019). HLA-DO modulates the diversity of the MHC-II self-peptidome. Mol. Cell. Proteomics *18*, 490–503.

Nanaware, P.P., Jurewicz, M.M., Clement, C.C., Lu, L., Santambrogio, L., and Stern, L.J. (2021). Distinguishing signal from noise in immunopeptidome studies of limiting-abundance biological samples: peptides presented by I-A(b) in C57BL/6 mouse thymus. Front. Immunol. *12*, 658601.

Nguyen, T.T., Klasener, K., Zurn, C., Castillo, P.A., Brust-Mascher, I., Imai, D.M., Bevins, C.L., Reardon, C., Reth, M., and Baumgarth, N. (2017). The IgM receptor FcmuR limits tonic BCR signaling by regulating expression of the IgM BCR. Nat. Immunol. *18*, 321–333.

Pham, T.D., Chng, M.H.Y., Roskin, K.M., Jackson, K.J.L., Nguyen, K.D., Glanville, J., Lee, J.Y., Engleman, E.G., and Boyd, S.D. (2017). High-fat diet induces systemic B-cell repertoire changes associated with insulin resistance. Mucosal Immunol. *10*, 1468–1479.

Pos, W., Sethi, D.K., and Wucherpfennig, K.W. (2013). Mechanisms of peptide repertoire selection by HLA-DM. Trends Immunol. *34*, 495–501.

Reyes-Vargas, E., Barker, A.P., Zhou, Z., He, X., and Jensen, P.E. (2020). HLA-DM catalytically enhances peptide dissociation by sensing peptide-MHC class II interactions throughout the peptide-binding cleft. J. Biol. Chem. *295*, 2959–2973.

Reynaud, C.A., Garcia, C., Hein, W.R., and Weill, J.C. (1995). Hypermutation generating the sheep immunoglobulin repertoire is an antigen-independent process. Cell *80*, 115–125.

Rodriguez-Zhurbenko, N., Quach, T.D., Hopkins, T.J., Rothstein, T.L., and Hernandez, A.M. (2019). Human B-1 cells and B-1 cell antibodies change with advancing age. Front. Immunol. *10*, 483.

Sanchez, M.L., Katsumata, K., Atsumi, T., Romero, F.I., Bertolaccini, M.L., Funke, A., Amengual, O., Kondeatis, E., Vaughan, R.W., Cox, A., et al. (2004). Association of HLA-DM polymorphism with the production of antiphospholipid antibodies. Ann. Rheum. Dis. *63*, 1645–1648.

Sette, A., Southwood, S., Miller, J., and Appella, E. (1995). Binding of major histocompatibility complex class II to the invariant chain-derived peptide, CLIP, is regulated by allelic polymorphism in class II. J. Exp. Med. *181*, 677–683.

Shaw, P.X., Goodyear, C.S., Chang, M.K., Witztum, J.L., and Silverman, G.J. (2003). The autoreactivity of anti-phosphorylcholine antibodies for atherosclerosis-associated neo-antigens and apoptotic cells. J. Immunol. *170*, 6151–6157.

Sloan, V.S., Cameron, P., Porter, G., Gammon, M., Amaya, M., Mellins, E., and Zaller, D.M. (1995). Mediation by HLA-DM of dissociation of peptides from HLA-DR. Nature *375*, 802–806.

Tang, C.A., Lee, A.C., Chang, S., Xu, Q., Shao, A., Lo, Y., Spalek, W.T., Pinilla-Ibarz, J.A., Del Valle, J.R., and Hu, C.A. (2021). STING regulates BCR signaling in normal and malignant B cells. Cell. Mol. Immunol. *18*, 1016–1031.

Thomsen, M.C., and Nielsen, M. (2012). Seq2Logo: a method for construction and visualization of amino acid binding motifs and sequence profiles including sequence weighting, pseudo counts and two-sided representation of amino acid enrichment and depletion. Nucleic Acids Res. *40*, W281–W287.

Tung, J.W., Mrazek, M.D., Yang, Y., Herzenberg, L.A., and Herzenberg, L.A. (2006). Phenotypically distinct B cell development pathways map to the three B cell lineages in the mouse. Proc. Natl. Acad. Sci. U S A *103*, 6293–6298.

Wang, H., and Clarke, S.H. (2004). Positive selection focuses the VH12 B-cell repertoire towards a single B1 specificity with survival function. Immunol. Rev. *197*, 51–59.

Wen, L., Shinton, S.A., Hardy, R.R., and Hayakawa, K. (2005). Association of B-1 B cells with follicular dendritic cells in spleen. J. Immunol. *174*, 6918–6926.

Won, W.J., and Kearney, J.F. (2002). CD9 is a unique marker for marginal zone B cells, B1 cells, and plasma cells in mice. J. Immunol. *168*, 5605–5611.

Yang, Y., Wang, C., Yang, Q., Kantor, A.B., Chu, H., Ghosn, E.E., Qin, G., Mazmanian, S.K., Han, J., and Herzenberg, L.A. (2015). Distinct mechanisms define murine B cell lineage immunoglobulin heavy chain (IgH) repertoires. Elife *4*, e09083.

Yin, L., Trenh, P., Guce, A., Wieczorek, M., Lange, S., Sticht, J., Jiang, W., Bylsma, M., Mellins, E.D., Freund, C., et al. (2014). Susceptibility to HLA-DM protein is determined by a dynamic conformation of major histocompatibility complex class II molecule bound with peptide. J. Biol. Chem. *289*, 23449–23464.

Zhang, R., Alt, F.W., Davidson, L., Orkin, S.H., and Swat, W. (1995). Defective signalling through the T- and B-cell antigen receptors in lymphoid cells lacking the vav proto-oncogene. Nature *374*, 470–473.

Zhou, Y., Li, Y.S., Bandi, S.R., Tang, L., Shinton, S.A., Hayakawa, K., and Hardy, R.R. (2015). Lin28b promotes fetal B lymphopoiesis through the transcription factor Arid3a. J. Exp. Med. *212*, 569–580.

Zhou, Z., Reyes-Vargas, E., Escobar, H., Rudd, B., Rockwood, A.L., Delgado, J.C., He, X., and Jensen, P.E. (2016). Type 1 diabetes associated HLA-DQ2 and DQ8 molecules are relatively resistant to HLA-DM mediated release of invariant chain-derived CLIP peptides. Eur. J. Immunol. *46*, 834–845.

Zhou, Z., Reyes-Vargas, E., Escobar, H., Chang, K.Y., Barker, A.P., Rockwood, A.L., Delgado, J.C., He, X., and Jensen, P.E. (2017). Peptidomic analysis of type 1 diabetes associated HLA-DQ molecules and the impact of HLA-DM on peptide repertoire editing. Eur. J. Immunol. *47*, 314–326.

STAR★METHODS

KEY RESOURCES TABLE

REAGENT or RESOURCE	SOURCE	IDENTIFIER
Antibodies		
Annexin V APC	Biolegend	Cat#640920; RRID: AB_2561515
B220 AF488	Biolegend	Cat#103228; RRID: AB_492874
B220 AF700	Biolegend	Cat#103231; RRID:AB_493716
B220 APC	Biolegend	Cat#103211; RRID: AB_493716
B220 PCPCy5.5	Biolegend	Cat#103235; RRID: AB_893356
B220 PE	Biolegend	Cat#103207; RRID: AB_312992
BrdU AF647	BD Bioscience	Cat#560209; RRID: AB_1645615
CD11b Biotin	Biolegend	Cat#101203; RRID: AB_312786
CD11b BV711	Biolegend	Cat#101241; RRID: AB_11218791
CD11b PCPCy5.5	Biolegend	Cat#101227; RRID: AB_893233
CD11c Biotin	Biolegend	Cat#117303; RRID: AB_313772
CD11c PCPCy5.5	Biolegend	Cat#117327; RRID: AB_2129642
CD19 BUV395	BD Bioscience	Cat#563557; RRID: AB_2722495
PE microbeads	Miltenyi biotec	Cat#130-048-801; RRID:AB_244373
CD19 PE	Biolegend	Cat#115507; RRID: AB_313642
CD19 BV650	Biolegend	Cat#115541; RRID: AB_11204087
CD21/35 Pacific Blue	Biolegend	Cat#123413; RRID: AB_2085159
CD23 BV510	BD Bioscience	Cat#563200; RRID:AB_2738064
CD3 Biotin	Biolegend	Cat#100243; RRID:AB_2563946
CD3 PCPCy5.5	Biolegend	Cat#100327; RRID:AB_893320
CD4 PCPCy5.5	Biolegend	Cat#116011; RRID:AB_2563022
CD43 FITC	Biolegend	Cat#143204; RRID:AB_10960745
CD43 PE-Cy7	Biolegend	Cat#143210; RRID:AB_2564349
CD45.1 BV650	BD Bioscience	Cat#563754; RRID:AB_2738405
CD45.1 PE	Biolegend	Cat#110708; RRID:AB_313497
CD45.2 AF700	Biolegend	Cat#109821; RRID:AB_493730
CD5 PCPCy5.5	Biolegend	Cat#100623; RRID:AB_2563432
CD5 PE-Cy5	Biolegend	Cat#100609; RRID:AB_312738
CD9 FITC	Biolegend	Cat#124807; RRID:AB_1279324
CD93 APC	Biolegend	Cat#136509; RRID:AB_2275879
CD93 PE-Cy7	Biolegend	Cat#136505; RRID:AB_2044011
I-Ab PE	Santa Cruz	Cat#sc-53946 PE; RRID:AB_831549
c-kit PE-Cy7	Biolegend	Cat$105813; RRID:AB_313222
Gr-1 Biotin	Biolegend	Cat#108403; RRID:AB_313368
Gr-1 PCPCy5.5	Biolegend	Cat#108427; RRID:AB_893561
H2-M Purified	BD Bioscience	Cat#552405; RRID:AB_394380
H2-M AF488	Fluorophore-conjugated using NHS ester (Invitrogen)	N/A
H2-M AF647	Fluorophore-conjugated using NHS ester (Invitrogen)	N/A
H2-O AF647	(Fallas et al., 2007)	N/A
I-A/I-E AF700	Biolegend	Cat#107622; RRID:AB_493727
I-A/I-E Biotin	Biolegend	Cat#107603; RRID:AB_313318
I-A/I-E BV605	Biolegend	Cat#107639; RRID:AB_2565894

(*Continued on next page*)

Continued

REAGENT or RESOURCE	SOURCE	IDENTIFIER
I-Ab Biotin	Biolegend	Cat#116403; RRID:AB_313722
I-Ab Purified	Biolegend	Cat#114402; RRID:AB_313577
I-Ad Biotin	Biolegend	Cat#115003; RRID:AB_313618
CD79a PE	Biolegend	Cat#133103; RRID:AB_1595633
CD79b FITC	Biolegend	Cat#132805; RRID:AB_2244530
IgD AF700	Biolegend	Cat#405729; RRID:AB_2563340
IgD BV510	Biolegend	Cat#405723; RRID:AB_2562742
IgA Biotin	Biolegend	Cat#407003; RRID:AB_315078
IgG PE/Dazzle 594	Biolegend	Cat#405330; RRID:AB_2566458
Ig-K BV421	BD Bioscience	Cat#562888; RRID:AB_2737867
Ig-l BV421	BD Bioscience	Cat#744523; RRID:AB_2742297
Ig-l PE	Biolegend	Cat#407307; RRID:AB_1027660
IgM AF488	Biolegend	Cat#406522; RRID:AB_2562859
IgM BV421	Biolegend	Cat#406532; RRID:AB_2650930
IgM BV605	Biolegend	Cat#406523; RRID:AB_2563358
Ig-M Purified	Biolegend	Cat#406501; RRID:AB_315051
I-Ab AF647	Biolegend	Cat#115309; RRID:AB_493139
NK1.1 PCPCy5.5	Biolegend	Cat#108727; RRID:AB_2132706
Nur77 PE	eBioscience	Cat#12-5965-80; RRID:AB_1257210
pAkt AF647	BD bioscience	Cat#560343; RRID:AB_1645397
pBtk BV421	BD bioscience	Cat#564848; RRID:AB_2738982
Phosphatidylcholine AF488	Established in Herzenberg lab	N/A
Sca-1 AF488	Biolegend	Cat#108115; RRID:AB_493270
Streptavidin BV605	Thermo fisher	C10103MP
Streptavidin Microbeads	Miltenyi biotec	Cat#130-048-102
Ter-119 PCPCy5.5	Biolegend	Cat#116227; RRID:AB_893638
Thy1.2 BV510	Biolegend	Cat#140319; RRID:AB_2561395
Fc block CD16/32	eBioscience	Cat#14-0161-82; RRID:AB_467133
Viable dye eFluor780	eBioscience	Cat#65-0865-14
Chemicals, peptides, and recombinant proteins		
Ig-k Purified	BD Bioscience	Cat#559749; RRID:AB_397313
I-Ab Purified (KH74)	Biolegend	Cat#115302; RRID:AB_313631
Anti-MHC class II Antibody (15G4)	Santa Cruz	Cat#sc-53946; RRID:AB_831549
Purified anti-mouse I-A/I-E Antibody	Biolegend	Cat#107601; RRID:AB_313316
Critical commercial assays		
RNeasy Mini Kit	QIAGEN	Cat# 74106
Duolink® In Situ Orange Starter Kit Mouse/Rabbit	Sigma-Aldrich	Cat# DUO92102
Phospho Antibody Array	Full Moon Biosystems	Cat# PTC188
Deposited data		
Mass spec data set	MassIVE data repository	MassIVE:MSV000087031 (https://doi.org/10.25345/C5S80D), MassIVE: MSV000088470 (https://doi.org/10.25345/C50G4V)
Ig repertoire analysis	Zenodo	Zenodo:5706066 (https://doi.org/10.5281/zenodo.5706066)

(*Continued on next page*)

Continued

REAGENT or RESOURCE	SOURCE	IDENTIFIER
Experimental models: Cell lines		
T2.DR3	(Denzin et al., 1994)	N/A
T2.DR3.DM	(Denzin et al., 1994)	N/A
Experimental models: Organisms/strains		
C57BL/6	The Jackson Lab	000664
B6.SJL-Ptprc^{a}Pepc^{b}/BoyJ	The Jackson Lab	002014
B6.129S2-H2$^{dlAb1\text{-}Ea}$/J	The Jackson Lab	003584
B6.129S7-Rag1^{tm1Mom}/J	The Jackson Lab	002216
Softwares and algorithms		
FlowJo 10.9	FlowJo	https://www.flowjo.com/
Prism 7	GraphPad	https://www.graphpad.com/
ImageJ – Fiji package	Freeware	https://fiji.sc/
Volocity 5.1	Quorum Technologies	https://quorumtechnologies.com/volocity/
IgBLAST	NCBI	https://www.ncbi.nlm.nih.gov/igblast/
MaxQuant	(Cox and Mann, 2008)	https://www.biochem.mpg.de/5111795/maxquant
GibbsCluster-2.0	(Andreatta et al., 2013)	http://www.cbs.dtu.dk/services/GibbsCluster-2.0
Seq2Logo 2.0	(Thomsen and Nielsen, 2012)	http://www.cbs.dtu.dk/biotools/Seq2Logo/
Oligonucleotides		
Primer sequence: *H2-DMa_Forward:* CTCG AAGCATCTACACCAGTG	This paper	N/A
Primer sequence: *H2-DMa_Reverse:* TCC GAGAGCCCTATGTTGGG	This paper	N/A
Primer sequence: *H2-DMb1_Forward:* ACCCCACAGGACTTCACATAC	This paper	N/A
Primer sequence: *H2-DMb1_Reverse:* GGATACAGCACCCCAAATTCA	This paper	N/A
Primer sequence: *H2-DMb2_Forward:* ACCTTTCTGGGATGTGCTGACC	This paper	N/A
Primer sequence: *H2-DMb2_Reverse:* GTGATGGTCACATCCGCTGGAT	This paper	N/A
Primer sequence: *H2-DOa_Forward:* GTCCCGGTACTCCTAACCGTA	This paper	N/A
Primer sequence: *H2-DOa_Reverse:* GCGTCGTAAGATTGGTAGAAGG	This paper	N/A
Primer sequence: *H2-DOb_Forward:* AGGCGGACTGTTACTTCACC	This paper	N/A
Primer sequence: *H2-DOb_Reverse:* ATCCAGGCGTTTGTTCCACTG	This paper	N/A
Primer sequence: *H2-Aa_Forward:* TCAGTCGCAGACGGTGTTTAT	This paper	N/A
Primer sequence: *H2-Aa_Reverse:* GGGGGCTGGAATCTCAGGT	This paper	N/A
Primer sequence: *H2-Ab1_Forward:* AAGGCATTTCGTGTACCAGTTC	This paper	N/A
Primer sequence: *H2-Ab1_Reverse:* CCTCCCGGTTGTAGATGTATCTG	This paper	N/A
Primer sequence: *Bmi1_Forward:* TGCAGATGAGGAGAAGAGGA	This paper	N/A

(*Continued on next page*)

Continued

REAGENT or RESOURCE	SOURCE	IDENTIFIER
Primer sequence: *Bmi1_Reverse:* TCATTCACCTCTTCCTTAGGC	This paper	N/A
Primer sequence: *Nr4a1_Forward:* TTGAGTTCGGCAAGCCTACC	This paper	N/A
Primer sequence: *Nr4a1_Reverse:* GTGTACCCGTCCATGAAGGTG	This paper	N/A
Primer sequence: *Ighv11_Forward:* GGGACTCTCTTGTGAAGGCTC	This paper	N/A
Primer sequence: *Ighv11_Reverse:* GCGTAGTTTATTGCACTGCCA	This paper	N/A
Primer sequence: *Ighv12-03_Forward:* CTGGTTTCCCCATCACCAGT	This paper	N/A
Primer sequence: *Ighv12-03_Reverse:* GATGGGGCTCTGGAGAGATG	This paper	N/A
Primer sequence: *Ighv1-55_Forward:* TGTTGGAGGATGTGTCTGCTG	This paper	N/A
Primer sequence: *Ighv1-55_Reverse:* GCACAGCTTCTGGCTTTAACA	This paper	N/A
Primer sequence: *Ighv6-06_Forward:* TAGTGACGCCTGGATGGACT	This paper	N/A
Primer sequence: *Ighv6-06_Reverse:* ATGCCAGTGTCTTCAGCTCTT	This paper	N/A
Primer sequence: *Rplp0_Forward:* TTTGACAACGGCAGCATT	This paper	N/A
Primer sequence: *Rplp0_Reverse:* ACCCTCCAGAAAGCGAGA	This paper	N/A

RESOURCE AVAILABILITY

Lead contact

Further information and requests for resources and reagents should be directed to and will be fulfilled by the Lead Contact, Elizabeth D. Mellins (mellins@stanford.edu).

Materials availability

This study did not generate new unique reagents.

Data and code availability

- The mass spec datasets presented in this study can be found in MassIVE data repository (http://massive.ucsd.edu) developed by Center for Computational Mass Spectrometry (University of California, San Diego) in MassIVE: MSV000087031 (I-A^b immunopeptidome from WT splenic B cells), and MassIVE: MSV000088470 (Total MHCII (M5/114), c1p/MHCII (KH74), and c2p/MHCII (15G4) immunopeptidome from WT and *H2-M*$^{-/-}$ B cells). The BCR repertoire dataset presented in this study can be found in Zenodo: 5706066 (https://doi.org/10.5281/zenodo.5706066) .
- This paper does not report original code.
- Any additional information required to reanalyze the data reported in this paper is available from the lead contact upon request.

EXPERIMENTAL MODEL AND SUBJECT DETAILS

Mice

Adult C57BL/6, B6.SJL-Ptprc^{a}Pepc^b/BoyJ (CD45.1$^+$) (002014), and B6.129S2-H2$^{dlAb1\text{-}Ea}$/J (MHCII deficient) (003584), B6.129S7-Rag1^{tm1Mom}/J (Rag1 deficient) (002216) mice were purchased from The Jackson Laboratory. H2-M and H2-O deficient mice in B6 background were a gift from Dr. Peter Jensen, University of Utah. H2-M deficient mice in BALB/c background were a gift from Dr. Laurence C Eisenlohr, University of Pennsylvania. All mice were housed, bred, and cared in specific-pathogen-free facilities at

Stanford Veterinary Service center at Stanford University, and all the experiments conformed to ethical principles and guidelines under the approval of the Administrative Panel for Laboratory Animal Care, protocol no. 33157. The mice were used at the ages specified for the experiments; for adults, 6-8 weeks old, equal distribution of both sex was ensured, whereas sex bias was ignored for experiments with neonatal mice. Mice aged 1, 2 or 3 weeks old were used for the neonatal studies.

Cell lines

The TxB hybrid APC cell lines T2.DR3 and T2.DR3.DM wild-type DR3 and DM have been established previously (Denzin et al., 1994) and were a gift from Dr. Lisa Denzin. They were cultured in complete RPMI (RPMI 1640 with 10% FBS, 1% non-essential amino acids, 1% sodium pyruvate, and 1% L-glutamate) and maintained at 37°C in a humidified atmosphere of 5% CO_2.

METHOD DETAILS

Flow cytometry

Single-cell suspensions were achieved by passing the spleen through a 40 μm cell strainer or flushing the bone marrow and peritoneum with RPMI media. The cell suspension was then treated with a 0.86% NH_4Cl solution for 10 min at room temperature to lyse erythrocytes, followed by re-suspension in complete RPMI (RPMI 1640 supplemented with 10% FBS, 1% non-essential amino acids, 1% sodium pyruvate, 1% L-glutamate, 1% penicillin-streptomycin, and 0.1% β-mercaptoethanol). Phenotypic analysis of cell populations was performed by staining single-cell suspensions with fluorochrome-conjugated or biotinylated monoclonal antibodies, followed by the acquisition of cells on an LSRII flow cytometer (BD at Stanford Shared FACS Facility) and analysis using FlowJo software (version 10.6.1, Treestar Inc.). Fluorescent-minus-one (FMO) controls were used to set the gates for negative populations, as well as for histograms representing background staining. Briefly, 3×10^6 cells were incubated with Fc block (10% 2.4G2 Fc block, 0.5% normal rat IgG, and 0.5% normal mouse IgG) in FACS buffer (0.2% BSA and 0.2% 0.5M EDTA in 1× PBS) for 10 min. The surface staining was performed using appropriate dilutions of antibodies in FACS buffer for 30 min at 4°C. For intracellular staining of pAkt, pBtk, pAkt, and Nur77, the Foxp3 fixation/permeabilization kit (eBioscience) was used; whereas intracellular CD79a (Ig-α), CD79b (Ig-β), H2-M and H2-O staining was performed using BD permeabilization buffer. BrdU staining was performed using the manufacturer's protocol (BD, catalog no. 552598).

Cell isolation

For sorting, single-cell suspensions from the spleen were enriched for Lin− cells, using biotinylated monoclonal antibodies against lineage markers (CD3e, Ter-119, CD11b, and CD11c), followed by incubation with streptavidin microbeads (Miltenyi) and negative selection using Magnetic-Activated cell sorting (MACS) on an LS magnetic column (Miltenyi #130-042-401). The lineage-negative fractions were subsequently stained with fluorochrome-conjugated antibodies to Lineage markers (Ter-119, CD3e, CD4, NK1.1, Gr-1, CD11b, and CD11c), CD19, CD43, CD5, CD21, and CD23. Dead cells (excluded by counterstaining with live/dead fixable dye; eBioscience) and doublets were gated out before sorting on a FACSAria (BD). Precursor B-1 cells and Mature B-1a cells were collected by sorting for $Lin^-Ig(\kappa/\lambda)^-CD19^+B220^{lo/-}CD93^+$ (Precursor B-1 cells) and $CD19^{hi}B220^{+/lo}CD93^-CD23^-CD21^-CD43^+CD5^+$ (Mature B-1a cells) populations. Additionally, during adoptive transfer experiments using donor mice, sorted cells were ensured for their expression of CD45.1 or CD45.2.

RNA extraction and qPCR

Splenic derived B-1 cell precursors, and mature B-1a cells were sorted into RNA lysis buffer (Qiagen), and RNA was isolated using an RNeasy mini kit following the manufacturer's protocol. The resulting RNA from each sample was DNase treated using RNase-free DNase (Promega), followed by cDNA preparation using iScript cDNA synthesis kit (Bio-Rad). For real-time quantitative RT-PCR, cDNA from an equivalent number of cells was mixed with SYBR Green master mix (Bio-Rad) and appropriate primer sets (provided in Table); analysis was performed using a CFX384 Touch Real-Time PCR Detection System and Bio-RAD CFX manager software. Relative expression was normalized to *Rplp0*.

Immunofluorescence

$CD19^+$ cells were MACS-enriched from spleen using biotinylated anti-CD19 antibody (6D5, BioLegend) and streptavidin microbeads (Miltenyi). A single-cell suspension was achieved by resuspending in PBS supplemented with 3% FCS and 0.2% 0.5M EDTA. 1×10^4 $CD19^+$ cells were embedded on slides using the cytospin machine. The cells were fixed on slides with 4% PFA for 15 min at room temperature and permeabilized with 1× perm wash buffer (BD Pharmingen). After blocking, sections were incubated with appropriate dilutions of fluorophore-conjugated primary Abs (eBioscience) overnight at 4°C. Slides were mounted with Prolong Gold Antifade reagent with DAPI (Thermofisher) and imaged using an Upright AxioImager Epifluorescence microscope (Zeiss).

ELISA

Capture-IgM antibody, Phosphatidylcholine (PtC) and phosphorylcholine (PC), and 4-Hydroxy-3-nitrophenylacetyl (NP)-conjugated BSA was used to coat high-binding Immulon 4 HBX plates (BioExpress) overnight at 4°C. After blocking in 5% FCS in 1× PBS, serially diluted serum was incubated on the plate, followed by incubation with HRP-conjugated IgM Ab (Southern Biotech). SureBlue

substrate (KPL) was added to detect the Ag-specific Abs. The wells were read at 450 nm on an Infinite M1000 microplate reader (Tecan).

In vivo adoptive cell transfer

For adoptive transfer experiments, sorted B-1 cell precursors or mature B-1a cells were resuspended in an appropriate volume of endotoxin-free, sterile PBS (Life Technologies). The cells were transferred into the venous sinus retro-orbitally following an anesthetization with isoflurane at a concentration of 1×10^4 cells per mouse or intraperitoneally at a concentration of 1×10^6 cells per mouse.

BrdU incorporation analysis

For BrdU incorporation studies, groups of wildtype and *H2-M*$^{-/-}$ mice (B6) received BrdU ad libitum in drinking water (0.8 mg/ml), supplemented with 1% sucrose for six days. For control, regular drinking water was provided.

In vitro stimulation and cell culture

FACS-sorted B-1 cell precursors and mature B-1a cells (as described above) were rested at 37°C for 45 min in 5% CO_2 before treating them with stimulants. Purified cells were cultured with 10 μg/ml anti-mouse Ig-κ (Biolegend), or 10 μg/ml anti-mouse MHCII (Invitrogen), diluted in complete medium (RPMI 1640 with 10% FBS, 1% non-essential amino acids, 1% sodium pyruvate, 1% L-glutamate, 1% penicillin-streptomycin) in 96-well round-bottom plates indicated time durations for detection of pAkt, pBtk, and Nur77. The flow-cytometry analysis was done for the detection of the phosphorylated form of the proteins. For the detection of the phosphorylated forms of several proteins associated with the BCR-signaling pathway, phosphor-antibody array (Full Moon Biosystems) was used following the manufacturer's protocol. Briefly, the cell lysates from the purified cell population were labeled with biotin. Following the blocking at room temperature for 45 min in an orbital-shaking condition, biotinylated proteins from the cell lysates were coupled for 1-2 h at room temperature in an orbital shaking condition. The array was developed using an appropriate dilution of AF647-conjugated streptavidin. The microslides were scanned using Genepix microarray scanner (Molecular Devices, San Jose, CA).

Immunoglobulin repertoire analysis

1. IgH amplification and sequencing IGH DNA libraries for sequencing were generated from cDNA prepared from total RNA isolated from mouse tissues. Multiplexed primers targeting the mouse framework region (FR) 1 of IGHV were used in PCR reactions with primers targeting each isotype (IgM, IgD, IgG, and IgA) that also included sequence barcodes to permit multiplexed sequencing of amplicon libraries as previously described (Pham et al., 2017). The first PCR step products included partial Illumina linker sequences encoded by the primers, and a second PCR step was used to complete the linker sequences. Gel electrophoresis with 1.5% agarose gel was used to verify product size. Amplicons were subsequently gel-extracted, pooled, quantitated, and sequenced with an Illumina MiSeq instrument using 2×300 cycle kit.
2. Analysis of IgH sequence data Paired-end sequences were merged, demultiplexed to determine sample assignment based on primer-encoded barcode sequences and trimmed of primer sequences. Next, the variable (IGHV), diversity (IGHD), and joining (IGHJ) gene segment identities in each rearrangement, as well as somatic mutations of germ-line gene segments, were identified using the IgBLAST program. The IgBLAST program was executed using default parameters and IMGT mouse germ-line reference datasets for the IGHD and IGHJ alignment (Giudicelli et al., 2005). Isotype identity was established by exact match to non-primer-encoded sequence within exon 1 of the sequenced constant region. CDR-H3 was determined as the sequence flanked on the 5' end by the FR3-CDR-H3 boundary as identified by IgBLAST, and on the 3' end by CDR-H3-FR4 boundary determined by position weight matrix search trained to identify the WGQG motif and sequence variants. To avoid over-interpretation of sequencing errors as somatic mutations in antibody gene rearrangements, a threshold of 1% mutation in the IGHV gene segment was used to distinguish mutated sequences from germ-line sequences. Exact match IgH nucleotide sequences from the same isotype and sample were collapsed into and analyzed as one read. For D20 value calculation, all IgH sequences from each mouse were grouped into clonotypes, defined as sequences having identical IGHV, identical IGHJ gene call, identical CDR-H3 nucleotide length, and ≥90% CDR-H3 nucleotide sequence similarity. For each mouse, we determined the smallest number of clones required to constitute at least 20% of the total number of reads within that mouse (clonotype D20 value). A similar Clonotype D20 analysis with more stringent grouping criteria (identical IGHV gene, IGHJ gene, and CDR3 amino acid sequence), was performed to obtain VDJ-CDR3aa D20 value.

Proximity ligation assay

For *in situ* PLA, CD19-enriched cells from spleens were settled on μ-Slide Angiogenesis chambers (ibidi) for 30 min at 37°C. Cells were fixed with 2% PFA for 20 min at room temperature, and the *in situ* PLA was performed following the manufacturer's protocol (Duolink® PLA Fluorescence Protocol, Sigma). Briefly, following the blocking at 37°C for 60 min, the cells were incubated with appropriate dilutions of primary antibodies (Rabbit anti-mouse IgM (Invitrogen), and mouse anti-mouse CLIP-I-A^b (15G4, Santacruz Biotech), or mouse anti-mouse I-A^b (KH74, BioLegend)) overnight at 4°C. Secondary PLA-PLUS and MINUS probes were used the following day at 37°C for one hour. This step was followed by ligation of the probes at 37°C for 30 min and subsequent amplification of

the signals at 37°C for 100 min. Cell layers in each chamber were mounted using Duolink® In Situ Mounting Medium with DAPI and imaged using BZ-X800 microscope (Keyence). For each experiment, at least 150 B cells from several images were analyzed (Volocity). For each sample, the PLA signal counts per cell were calculated; co-localization of the confocal images of nuclei (DAPI, 405 nm laser) and PLA signal (568 nm laser) were analyzed for 50 cells per image with Volocity.

Immunoblot analysis

For Western blot analysis, cells were lysed in RIPA buffer with 1 mM PMSF and protease inhibitor cocktail. Protein concentration was determined using the Pierce Coomassie Plus Assay. Protein samples were resolved by SDS-PAGE and transferred to a PVDF membrane (0.45 μm). The following antibodies were used (at the indicated dilutions), Btk (1:2,000), phospho-Btk (1:1,000), Syk (1:2,000), phospho-Syk (1:1,000), IκBα (1:2,000), beta-Actin (1:5,000). Secondary antibodies were used at 1:5,000 dilution. Protein bands were visualized using ECL detection reagent.

Immunopeptidome analysis

For isolation of I-A^b peptide complexes we used a sequential immunoaffinity chromatography protocol previously developed for isolation of MHC class II peptides (Gorga et al., 1987; Nanaware et al., 2019, 2021). The splenic B cells from C57BL/6 WT and *H2-M*$^{-/-}$ mice were resuspended in 50 mM Tris-HCl, 150 mM NaCl, pH 8.0, containing protease inhibitor cocktail (Sigma-P2714) and 5% β-octylglucoside, freeze-thawed for 5-6 times. The lysate was spun at 4000×g for 5 min at 4°C to remove the cellular debris. The supernatant was collected and further spun using ultracentrifuge at 100,000 × g for 1 h at 4°C. The supernatant was used for the isolation of the MHCII-peptide complexes using an immunoaffinity column of M5/114, KH74, or 15G4 monoclonal antibodies immobilized onto CNBr-activated Sepharose CL-4B. The lysates were pre-cleared sequentially with CNBr activated Sepharose beads only, followed by isotype control antibody-conjugated beads, and rotated slowly on a shaker for 1 h at 4°C to remove proteins binding nonspecifically to beads or antibodies. This equilibrated lysate was removed from the beads and then further sequentially incubated with KH74 antibody-conjugated beads, and then with 15G4 antibody-conjugated beads, rotated slowly each time for 2 h on a shaker at 4°C. The column was washed by passing several buffers in succession as follows: (1) 50 mM Tris-HCl, 150 mM NaCl, pH 8.0, containing protease inhibitors and 5% β-octylglucoside (5 times the bead volume); (2) 50 mM Tris-HCl, 150 mM NaCl, pH 8.0, containing protease inhibitors and 1% β-octylglucoside (10 times the bead volume); (3) 50 mM Tris-HCl, 150 mM NaCl, pH 8.0, containing protease inhibitors (30 times the bead volume); (4) 50 mM Tris-HCl, 300 mM NaCl, pH 8.0, containing protease inhibitors (10 times the bead volume); (5) 1X PBS (30 times the bead volume); and (6) HPLC water (100 times the bead volume). Similarly, pre-cleared lysate from *H2-M*$^{-/-}$ mice were incubated separately with M5/114 antibody-conjugated beads and washed as described above. Peptides were eluted from the washed resins using a 2% TFA solution. Eluted peptide mixtures were then separated from I-A^b proteins, residual detergent, and cellular material by binding to a Vydac C18 macrospin column (The Nest Group, USA). and eluting with 30% acetonitrile containing 0.1% (v/v) TFA. The solvent was removed by Speed-Vac and the dried peptide extracts were stored at -80°C or used immediately. I-A^b-eluted peptides were resuspended in 10μL of 3% ACN/0.1% formic acid and analyzed using a Thermo Scientific Orbitrap Fusion Tribrid mass spectrometer. The peptides were identified by processing the raw ion fragmentation spectra using MaxQuant (Cox and Mann, 2008) against the combined database of UniProt_Mouse, which was downloaded on 10/7/16 with 57,984 entries. Search parameters included "no enzyme" specificity to detect peptides generated by "cleavage" after any residue. The variable modifications of oxidized methionine and pyroglutamic acid for N-terminal glutamine were considered. The peptides identified in the beads only and isotype antibody-conjugated beads were considered as non-specific peptides and excluded from the analysis. All identified peptides >11 residues were included in the analysis. For some analyses, MHC-binding cores were identified for each peptide using NetMHCIIpan3.2, and peptides of different lengths sharing the same core (nested sets) were considered together. GibbsCluster-2.0 server (Andreatta et al., 2013) was used to identify the motif for the eluted peptides and were displayed by Seq2Logo 2.0 (Thomsen and Nielsen, 2012). The eluted peptide sequences were aligned using the preference for hydrophobic residue at P1 position and clustering sequence weighing algorithm to identify the motif with the length of 9 amino acids (Nanaware et al., 2021).

QUANTIFICATION AND STATISTICAL ANALYSIS

One-way analysis of variance (ANOVA) was used for comparing data obtained from three or more groups of mice, followed by Kruskal-Wallis test for multiple comparisons between the groups; whereas two-way ANOVA was used for comparison between two or more groups, followed by Bonferroni's test for multiple comparisons between the groups, unless otherwise mentioned. For analysis between two groups of mice non-parametric Mann-Whitney's U-test was performed. All the statistical analysis was performed using Prism 8.0 (GraphPad Software, Inc., San Diego, CA).